



**UNIVERSIDADE FEDERAL DE ALAGOAS
INSTITUTO DE FÍSICA**

ALVARO HERRERA CARRILLO

**OPTICAL CHARACTERIZATION AND STUDY OF THE JUDD-OFELT
PARAMETERS OF Nd³⁺ AND Sm³⁺ IONS IN DIFFERENT GLASSES AND CRYSTALS
FOR PHOTONIC APPLICATIONS**

Maceió

2012



UNIVERSIDADE FEDERAL DE ALAGOAS
INSTITUTO DE FÍSICA

ALVARO HERRERA CARRILLO

**OPTICAL CHARACTERIZATION AND STUDY OF THE JUDD-OFELT
PARAMETERS OF Nd³⁺ AND Sm³⁺ IONS IN DIFFERENT GLASSES AND CRYSTALS
FOR PHOTONIC APPLICATIONS**

Dissertation submitted to the Instituto de Física of the
Universidade Federal de Alagoas in partial fulfillment
of the requirements for the degree of Master in Science.

Supervisor: Prof. Dr. Carlos Jacinto Da Silva

Maceió

2012

Catálogo na fonte
Universidade Federal de Alagoas
Biblioteca Central
Divisão de Tratamento Técnico

Bibliotecária responsável: Fabiana Camargo dos Santos

H564o Herrera Carrillo, Alvaro.

Optical characterization and study of the Judd-Ofelt parameters of Nd³⁺ and Sm³⁺ ions in different glasses and crystals for photonics applications / Alvaro Herrera Carrillo. – 2012.

117 f. : il.

Orientador: Carlos Jacinto da Silva.

Dissertação (Mestrado em Física) – Universidade Federal de Alagoas. Instituto de Física. Maceió, 2012.

Bibliografia: f. 112-117.

1. Judd-Ofelt – Teoria. 2. Vidros. 3. Cristais. I. Título.

CDU: 535.343.2

**PARECER DA BANCA EXAMINADORA DE DEFESA DE
DISSERTAÇÃO DE MESTRADO**

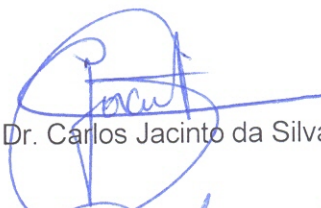
“Optical Characterization and study of the Judd-Ofelt parameters of Nd³⁺ and Sm³⁺ ions in different glasses and crystals for photonic applications”.

por

Álvaro Herrera Carrillo

A Banca Examinadora composta pelos professores Carlos Jacinto da Silva (orientador), do Instituto de Física da Universidade Federal de Alagoas, Andrea Simone Stucchi de Camargo, do Instituto de Física de São Carlos da Universidade de São Paulo, e Wagner Ferreira da Silva, do Instituto de Física da Universidade Federal de Alagoas consideram o candidato aprovado com grau “ A ”.

Maceió, 03 de agosto de 2012



Prof. Dr. Carlos Jacinto da Silva



Profa. Dra. Andrea Simone Stucchi de Camargo



Prof. Dr. Wagner Ferreira da Silva

ACKNOWLEDGEMENTS

To God that always full of wisdom every corner of my universe.

To my dear parents, for their invaluable love, for guiding me spiritually to this new chapter of my life.

To my son Juan Sebastian, result of great inspiration and light of my life.

To my brothers for their constant emotional support.

I extend my sincerest gratitude to my supervisor, PhD. Carlos Jacinto for his leadership, patience, and encouragement throughout the course of this research as well as his invaluable assistance for finalizing this dissertation .

I wish to thank the staff in the Instituto de Física of Universidade Federal de Alagoas. Your help, assistance and friendship made working at the university a pleasure.

Thanks to members of the group GFFC, especially for teachers Maria Tereza and Marcos Vermelho for his entire confidence and constant support for the development of this research.

My sincere thanks to the providers of some samples: Instituto de Física de São Carlos-USP- Prof. Dr. A. S. S. de Camargo, Universidade Federal do Ceará – Prof. Dr. Ilde Guedes, Kigre Inc., Hilton Head, Instituto de Física de São Carlos USP- Prof. Dr. A. C. Hernandez, Universidade Estadual de Maringá – Prof. Dr. Mauro L. Baesso, Universidade Federal de Uberlândia – Prof. Dr. Noélio Oliveira Dantas, Universidade Autônoma de Madrid – Prof. Dr. Daniel Jaque.

I wish to thank my friends and colleagues who have made this journey more enjoyable than I could have imagined. In particular, I would like to thank Eliel, Marlon, Tarita and Kisie for the good times and late nights spent at University. The many helpful discussions and bohemian nights were much appreciated.

Finally, to CNPq for its financial support to complete this new phase of knowledge.

ABSTRACT

In this work, a set of Sm^{3+} and Nd^{3+} doped samples was investigated using spectroscopic technique and the Judd-Ofelt theory. Precisely, investigations were carried out on the glasses $\text{Sm}:\text{InSrBaZnGdNa}$, $\text{Sm}:\text{InSrBaZnGdNaPO}$, $\text{Sm}:\text{BPbGeBi}$, $\text{Nd}:\text{Q-98}$, $\text{Nd}:\text{Q-100}$, $\text{Nd}:\text{YALB}$, $\text{Nd}:\text{LSCAS}$, $\text{Nd}:\text{BNaPbAl}$, $\text{Nd}:\text{BNaPbAlTi}$, $\text{Nd}:\text{YAG}$ ceramics, and $\text{Nd}:\text{YVO}_4$ and GdVO_4 crystals. Using Judd-Ofelt theory, various parameters such as transition probabilities A_{ij} , radiative lifetimes τ_R , and calculated branching ratios β_{ij} were obtained. By the Ω_λ ($\lambda = 2, 4$ and 6) intensity parameters, we concluded what are the best systems, among the investigated, for specific proposes. The variation in Ω_2 was discussed in terms of the covalent nature of the interaction between RE^{3+} (Nd^{3+} , Sm^{3+}) ions and the ligand field of the host matrix. The parameter Ω_4 presents a completely random behavior with the matrix being, therefore, not easy to understand it. Reasonably higher radiative property of ${}^4\text{G}_{5/2} \rightarrow {}^6\text{H}_{7/2}$ transition suggests that the $\text{Sm}:\text{InSrBaZnGdNa}$, $\text{Sm}:\text{InSrBaZnGdNaPO}$, and $\text{Sm}:\text{BPbGeBi}$ glasses are good candidates for reddish-orange laser applications. The radiative transitions rates (A_{rad}), branching ratio ($\beta_{JJ'}$), and radiative lifetime (τ_{rad}) were calculated for all the studied systems. The results obtained could be utilized to determine the potential applications of glass and crystal in optical devices and lasers.

Keywords: Judd-Ofelt theory, glasses, crystals, spectroscopy

RESUMO

Neste trabalho, um conjunto de amostras dopadas com Sm^{3+} e Nd^{3+} foi investigado usando técnica espectroscópica e a teoria de Judd-Ofelt. Precisamente, investigações foram realizadas nos vidros $\text{Sm}:\text{InSrBaZnGdNa}$, $\text{Sm}:\text{InSrBaZnGdNaPO}$, $\text{Sm}:\text{BPbGeBi}$, $\text{Nd}:\text{Q-98}$, $\text{Nd}:\text{Q-100}$, $\text{Nd}:\text{YALB}$, $\text{Nd}:\text{LSCAS}$, $\text{Nd}:\text{BNaPbAl}$, $\text{Nd}:\text{BNaPbAlTi}$, na cerâmica de $\text{Nd}:\text{YAG}$, e nos cristais de $\text{Nd}:\text{YVO}_4$ e GdVO_4 . Por meio da teoria de Judd-Ofelt foram obtidos vários parâmetros tais como probabilidades de transição A_{ij} , tempos de vida radiativo τ_R e razões de ramificação β_{ij} . Analisando os parâmetros de intensidade Ω_λ ($\lambda = 2, 4$ and 6) nós conseguimos concluir quais são os melhores sistemas, dentre os estudados, para propósitos específicos. A variação observada em Ω_2 foi discutida em termos da natureza covalente das interações entre o íon terra-rara (Nd^{3+} , Sm^{3+}) e o campo ligante da matriz hospedeira. O parâmetro Ω_4 apresentou um comportamento completamente aleatório para diferentes matrizes sendo, portanto, de difícil compreensão. A transição radiativa ${}^4\text{G}_{5/2} \rightarrow {}^6\text{H}_{7/2}$ sugere que os sistemas vítreos $\text{Sm}:\text{InSrBaZnGdNa}$, $\text{Sm}:\text{InSrBaZnGdNaPO}$ e $\text{Sm}:\text{BPbGeBi}$, são bons candidatos para aplicações lasers na região laranja-vermelho do espectro eletromagnético. As taxas de transição radiativas (A_{rad}), razão de ramificação ($\beta_{JJ'}$) e tempo de vida radiativo (τ_{rad}), foram calculados para todos os sistemas estudados. Os resultados obtidos podem ser utilizados para determinar o potencial de aplicações de vidros e cristais em dispositivos ópticos e lasers.

Palavras chave: Teoria de Judd-Ofelt, vidros, cristais, espectroscopia.

“Estamos en los primerísimos comienzos de la raza humana. No es irrazonable que tropecemos con problemas. [...] Nuestra responsabilidad como científicos, sabedores del gran progreso y el gran valor de una filosofía satisfactoria de la ignorancia, del gran progreso que es el fruto de la libertad de pensamiento, está en proclamar el valor de esta libertad, enseñar que la duda no debe ser temida, sino bienvenida y discutida, y exigir esta libertad como nuestro deber para con todas las generaciones venideras.”

Richard P. Feynman

TABLE OF CONTENTS

GENERAL INTRODUCTION	17
OBJETIVES	18
1 OVERVIEW ABOUT GLASSES AND CRYSTALS	19
1.1 The glassy state	19
1.2 Host glass	21
1.3 Photonic glasses and crystals	23
1.3.1 Silica glasses	23
1.3.2 Phosphate glasses	23
1.3.3 Low silica calcium aluminosilicate glass	24
1.3.4 Lead indium phosphate	25
1.3.5 Borates glasses	25
1.3.6 Fluoroindate glasses	26
1.3.7 Neodymium-doped yttrium aluminum garnet, Nd:YAG crystal	26
1.3.8 Yttrium Vanadate (YVO_4) cristal	27
1.3.9 Gadolinium Orthovanadate ($GdVO_4$) crystal	27
2. SPECTROSCOPIC PROPERTIES OF SOLIDS	29
2.1 Introduction to spectroscopic models	29
2.2 General considerations of the optical properties of rare earth ions	34
2.3 Optical properties of free ions	38
2.4 Energy levels	40
2.5 Optical properties of trivalent ions in crystalline and amorphous solids	51

3 JUDD-OFELT THEORY	56
3.1 Introduction to the Judd-Ofelt theory	56
3.2 Hypothesis of the Judd-Ofelt theory	57
3.3 Quantitative analysis of Judd-Ofelt theory	58
4 EXPERIMENTAL DETAILS	63
4.1 InSrBaZnGdNaSm and InSrBaZnGdNaSmPO glasses doped with Sm ³⁺ ion: influence of P ₂ O ₅ in fluoroindate glass	65
4.1.1 Radiative properties of Sm:InSrBaZnGdNaPO and Sm:InSrBaZnGdNa glasses	70
4.2 Sm ³⁺ doped BPbGeBi glass	71
4.2.1 Radiative properties of Sm ³⁺ DOPED BPbGeBi GLASS	74
4.3 Results and discussions	74
4.4 Conclusions	80
4.5 Analysis of the Judd-Ofelt parameters and radiative properties of Nd ³⁺ doped in glasses and crystal	82
4.5.1 Study of absorption spectra and calculation of Judd-ofelt parameters in different Nd ³⁺ doped glasses	85
4.5.2 Radiative properties of Nd ³⁺ doped PbInPO ₄ , InSrBaZnGdNa, Q-98,LSCAS, YALB, BNaPbAl, BNaPbAlTi, and Q-100 glasses	92
4.5.3 Results and discussions	94
4.5.2 Study of absorption spectra and calculation of Judd-Ofelt parameters Nd:YVO ₄ , Nd:GdVO ₄ , crystals and Nd: ceramics	98
4.5.2.1 Nd:YVO ₄ crista	99
4.5.2.2 Nd:GdVO ₄ crystal and Nd:YAG ceramic	101
4.5.3 Results and discussions	106
4.5.4 Conclusions	107

5 GENERAL CONCLUSIONS AND PROPOSED FUTURE	109
5.1 Conclusions	109
5.2 Proposed future	110
REFERENCES	112

LIST OF FIGURES

Figure 1.1 Glass and crystalline formation as a function of temperature	20
Figure 1.2 a) Diffraction patterns from a crystal, b) diffraction patterns of a glass, c) SEM micrographs for a crystal and d) glass	21
Figure 1.3 Energy level diagram of a Nd:YAG laser	28
Figure 2.1 Transitions of spectral series	30
Figure 2.2 Dieke diagram for energy levels of lanthanide ions in LaCl_3	53
Figure 2.3. Schema diagram of splitting of the energy levels of rare earth ions due to the different interactions	55
Figure 4.1 Absorption spectra of 2.0 mol % of Sm^{3+} doped $\text{Sm}:\text{InSrBaZnGdNa}$ and $\text{Sm}:\text{InSrBaZnGdNaPO}$	67
Figure 4.2 Shift of transitions due to the nephelauxetic effect	69
Figure 4.3 Optical absorption spectra of Sm^{3+} doped BPbGeBi glass	72
Figure 4.4 Hipersensitive transitions for $\text{Sm}:\text{BPbGeBi}$ and $\text{Sm}:\text{InSrBaZnGdNa}$	75
Figure 4.5 Ω_2 as a function of the glassy matrix	78
Figure 4.6 Ω_4 as a function of the glassy matrix	78

Figure 4.7 Ω_6 as a function of the glassy matrix	79
Figure 4.8 Ω_2 in function of the different glasses	79
Figure 4.9 (a) $\bar{\beta}$ and (b) δ parameters as a function of the Ω_2 parameter	80
Figure 4.10 Radial wave functions of the 4f, 5s, 5p and 6s shells for Nd ³⁺ ion	82
Figure 4.11 a) Engineering and b) atomistic representations of flash-lamp pumping, Nd ³⁺ excitation, and stimulated emission (amplification) in Nd ³⁺ -doped laser	84
Figure 4.12 Four-level system in Nd: YAG	85
Figure 4.13 Absorption spectra of Nd:PbInPO ₄ , Nd:InSrBaZnGdNa, Nd:Q-98, and Nd:LSCAS glasses	86
Figure 4.14 Absorption spectra of Nd:YALB, Nd:BNaPbAl, Nd:BNaPbAlTi, and Nd:Q- 100 glasses	86
Figure 4.15 Hypersensitive transitions observed for Nd:PbInPO ₄ , Nd:InSrBaZnGdNa, Nd:Q-98, and Nd:LSCAS glasses	95
Figure 4.16 δ versus Ω_2 Judd-Ofelt parameter for four Nd ³⁺ doped Glasses	97
Figure 4,17 Absorption spectrum of Nd: YVO ₄	99
Figure 4.18 Absorption spectra of Nd: YAG ceramic and Nd: GdVO ₄ crystal	102
Figure 4.19 Absorption band for the transition $^4I_{9/2} \rightarrow ^4G_{5/2}$ for Nd.YVO ₄ and Nd:GdVO ₄ and Nd: YAG crystal	106

LIST OF TABLES

Table 2.1 Spectral series	30
Table 2.2 Characteristics of lanthanide ions	39
Table 4.1 family of glasses and crystals with their respective acronyms and concentration % mol of earth rare (Nd³⁺, Sm³⁺)	64
Table 4.2 Linear refractive index and mass density for Sm:InSrBaZnGdNa Sm:InSrBaZnGdNaPO glasses	66
Table 4.3 Calculated and experimental oscillator strengths for Sm³⁺ doped InSrBaZnGdNa and InSrBaZnGdNaPO glasses	68
Table 4.4 Energy levels assignments and matrix elements for Sm:InSrBaZnGdNaPO and Sm:InSrBaZnGdNa glasses	69
Table 4.5 Intensity parameters $\Omega_\lambda (\times 10^{-20})(\lambda = 2,4,6)$ and quality factor Ω_4 / Ω_6 for Sm:InSrBaZnGdNa and Sm:InSrBaZnGdNaPO glasses	70
Table 4.6 Radiative decay rates $A_{rad}(s^{-1})$, branching ratio β_{rad}, and radiative lifetime $\tau_r(ms)$ for the main emitting states of Sm³⁺ doped InSrBaZnGdNa and InSrBaZnGdNaPO glasses	70
Table 4.7 Energy levels assignments and matrix elements for Sm:BPbGeBi glass	72

Table 4.8 The experimental and calculated oscillator strengths for Sm^{3+} ions in BPbGeBi	73
Table 4.9 Intensity parameters Ω_{λ} ($\times 10^{-20}$) ($\lambda = 2, 4, 6$) and quality factor Ω_4/Ω_6 for Sm^{3+} doped BPbGeBi glasses	73
Table 4.10 Radiative decay rates $A_{rad}(s^{-1})$, branching ratio β_{rad}, and radiative lifetime $\tau_r(ms)$ for the main emitting states of Sm^{3+} doped BPbGeBi glass	74
Table 4.11 Values for the Ω_{λ} ($\lambda = 2, 4, 6$) parameters and rigidity Ω_4/Ω_6 parameter for glasses studied in this work and some reported in the literature	76
Table 4.12 Values of $\bar{\beta}$ and δ for Sm^{3+} doped glasses	77
Table 4.13 Terms for each angular momentum quantum number J	83
Table 4.14 Maximum multiplicity for each term	84
Table 4.15 J' states and matrix elements for Nd^{3+} ions and used in the Nd:PbInPO₄, Nd:InSrBaZnGdNa, Nd:Q-98, Nd:LSCAS, Nd:YALB, and Nd:Q-100 glasses	87
Table 4.16 J' states and matrix elements for Nd:BNaPbAl and Nd:BNaPbAlTi glasses	88
Table 4.17 Energy (cm^{-1}), experimental, and calculated oscillator strengths ($\times 10^{-6}$) for Nd:PbInPO₄ glass	88
Table 4.18 Energy (cm^{-1}), experimental, and calculated oscillator strengths ($\times 10^{-6}$) for Nd:InSrBaZnGdNa glass	89

Table 4.19 Energy (cm^{-1}), experimental and calculated oscillator strengths ($\ast 10^{-6}$) for Nd:Q-98 glass	89
Table 4.20 Energy (cm^{-1}), experimental, and calculated oscillator strengths ($\ast 10^{-6}$) for Nd:LSCAS glass	90
Table 4.21 Energy (cm^{-1}), experimental, and calculated oscillator strengths ($\ast 10^{-6}$) for Nd:YALB glass	90
Table 4.22 Energy (cm^{-1}), experimental, and calculated oscillator strengths ($\ast 10^{-6}$) for Nd:BNaPbAl glass	91
Table 4.23 Energy (cm^{-1}), experimental, and calculated oscillator strengths ($\ast 10^{-6}$) for Nd:BNaPbAlTi glass	91
Table 4.24 Energy (cm^{-1}), experimental, and calculated oscillator strengths ($\ast 10^{-6}$) for Nd:Q-100 glass	92
Table 4.25 Judd-Ofelt parameters ($\Omega_{\lambda} \times 10^{-20} \text{cm}^2$), spectroscopy quality factor Ω_4/Ω_6 for Nd³⁺ doped PbInPO₄, InSrBaZnGdNa, Q-98, LSCAS, YALB, BNaPbAl, BNaPbAl, and Q-100 glasses	92
Table 4.26 Radiative properties such as radiative transitions rates A_{rad} (s^{-1}), radiative lifetime τ_{rad} (μs), and emission branching ratio β_{JJ} for Nd doped glasses	93
Table 4.27 Values of δ bonding parameter and Ω_2 Judd-Ofelt parameter for some Nd³⁺ doped glasses	96
Table 4.28 Experimental and calculated oscillator strengths ($\ast 10^{-6}$) for Nd:YVO₄ crystal	100

Table 4.29 Judd-Ofelt parameters ($\Omega_\lambda \times 10^{-20} \text{ cm}^2$) and the spectroscopic quality factor ($\frac{\Omega_4}{\Omega_6}$) for Nd:YVO₄	100
Table 4.30 Radiative properties such as radiative transitions rates A_{rad} (s^{-1}), radiative lifetime τ_{rad} (μs), and emission branching ratio β_{JJ} for Nd:YVO₄	100
Table 4.31 Energy values, J' states, oscillator strength and matrix elements for Nd: GdVO₄	103
Table 4.32 Experimental and calculated oscillator strengths ($*10^{-6}$) for Nd: GdVO₄	103
Table 4.33 Judd-Ofelt parameters ($\Omega_\lambda \times 10^{-20} \text{ cm}^2$) and the spectroscopic quality factor ($\frac{\Omega_4}{\Omega_6}$) for Nd: GdVO₄ crystal	104
Table 4.34 Radiative properties such as radiative transitions rates A_{rad} (s^{-1}), radiative lifetime τ_{rad} (μs), and emission branching ratio β_{JJ} for Nd: GdVO₄ crystal	104
Table 4.35 Energy values, J' states, oscillator strength and matrix elements for Nd:YAG Ceramic	104
Table 4.36 Experimental and calculated oscillator strengths ($*10^{-6}$) for NdYAG Ceramic	105
Table 4.37 Judd-Ofelt parameters ($\Omega_\lambda \times 10^{-20} \text{ cm}^2$) and the spectroscopic quality factor ($\frac{\Omega_4}{\Omega_6}$) for Nd³⁺ for Nd:YAG Ceramic	105

Table 4.38 Radiative properties such as radiative transitions rates A_{rad} (s^{-1}), radiative lifetime τ_{rad} (μs), and emission branching ratio β_{JJ} for Nd:YAG ceramic

105

GENERAL INTRODUCTION

In recent decades have been studied crystals and glasses doped with lanthanide ions to be exploited in a variety of photonic applications such as optical fibers, fluorescent devices, detectors, optical waveguides, and several other applications. The spectral properties of these ions in glasses and crystals vary in a wide range since they depend on the chemical composition.

The techniques used to the abovementioned studies are innumerable and the main of them is the optical spectroscopy of luminescence and absorption. Based on absorption bands of intra configurational $f-f$ transitions, the energy level intensities of trivalent Rare-Earth (RE^{3+}) ions, several host media were described and estimated quantitatively by using the Judd-Ofelt theory.^{1,2} This theory describes forbidden-parity transitions in RE ions in sites with no symmetry inversion and was developed within the formalism of tensor operators, $n-j$ symbols and reduced matrix elements..In the Judd-Ofelt theory the transition probability between any pair of Stark sublevels of the RE ion activator in $4f^N$ configuration can be written in terms of three phenomenological parameters called Ω_λ ($\lambda = 2,4,6$), which are known as Judd-Ofelt parameters. These parameters are determined experimentally by means of an adjustment of the intensities of the lines with corresponding theoretical and experimental lines registered in the absorption spectrum.

Large numbers of authors have conducted studies to attempt to explain the behavior of these parameters, for example, according to Jorgensen³ Ω_2 exhibits the dependence on the covalence between RE^{3+} ions and ligands anions, since Ω_2 reflects the asymmetry of the local environment at the RE^{3+} ion site, and thus Ω_2 is very small for ionic materials, such as fluorides, and quite large for covalent materials, such as silicates. On the other hand, Ω_4 and Ω_6 are related to the rigidity of the matrix. These intensity parameters are used to calculate the spontaneous emission probability ($A_{JJ'}$), lifetime radiative (τ_{rad}). Another factor that has an important influence on the performance of a device is the branching ratio ($\beta_{JJ'}$) for a transitions J to J' , defined as the fraction of all spontaneous decay processes that occur through that channel⁴.

OBJECTIVES

1. Analyses of the optical transitions of Sm^{3+} doped fluoroindate and fluoroindate modified with phosphorus pentoxide glasses. In the same manner, analyses of the optical transitions of Nd^{3+} doped in a variety of glasses and crystals in terms of the uniform free-ion Hamiltonian (\mathcal{H}_{FI}) model in which the parameters may be related to specific types of interactions.
2. Evaluate the Judd-Ofelt parameters Ω_λ from the measured oscillator strength for Sm^{3+} in glasses and Nd^{3+} in different glasses and crystals.
3. Discuss changes in the parameters Ω_λ of the Sm^{3+} and Nd^{3+} ions as a function of different host materials.
4. Evaluate and discuss the $A_{JJ'}$, $\beta_{JJ'}$ and τ_R parameters for fluorescent levels of Sm^{3+} and Nd^{3+} in different compounds in view of similar results reported in previous literatures.

1 OVERVIEW ABOUT GLASSES AND CRYSTALS

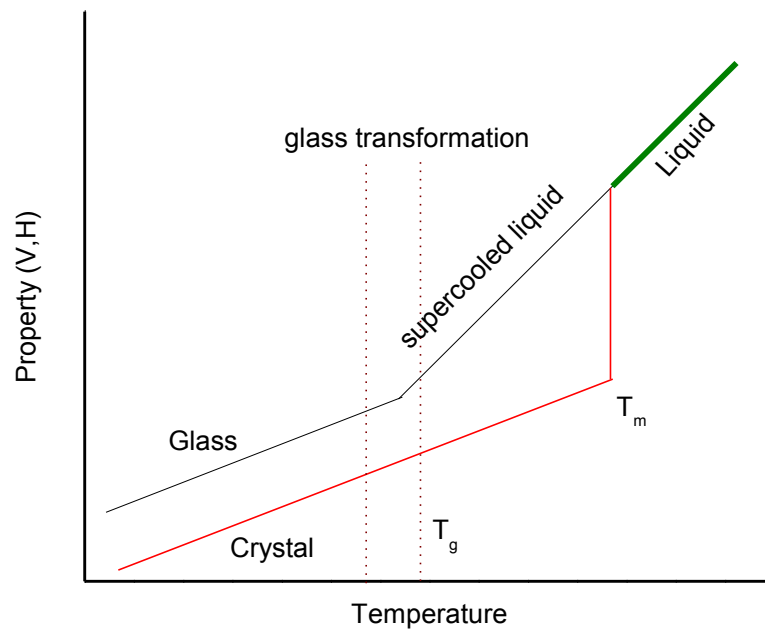
1.1 The glassy state

Most people associate the term glass with transparent materials manufactured from silicon oxide,^{5,6} however, under this concept we can include a large amount of amorphous materials, both organic and inorganic, such as is the case of polymers, semiconductors, and even sugars.

Summarizing, we can define a glass as a liquid that has lost its ability to flow, or as an amorphous solid material with structural characteristics of liquid, which has a glass transition. The easiest way to form a glass is cool it from its liquid state fast enough to avoid the occurrence of crystallization. To understand the transformation from liquid to glass we can monitor the volume changes as a function of temperature. Figure 1.1 shows that, by lowering the temperature of a liquid, two things can happen:

- 1) If the liquid crystallizes, there is a discontinuity at the melting temperature (dotted line), corresponding to a transformation of first order.
- 2) If the crystallization is "ignored", the liquid becomes supercooled metastable state and the curve remains the same slope. By continuing the cooling comes a time when the slope of the curve has a change, this temperature is called the glass transition temperature (T_g) and is the temperature at which the glass is formed.

Figure 1.1 Glass and crystalline formation as a function of temperature



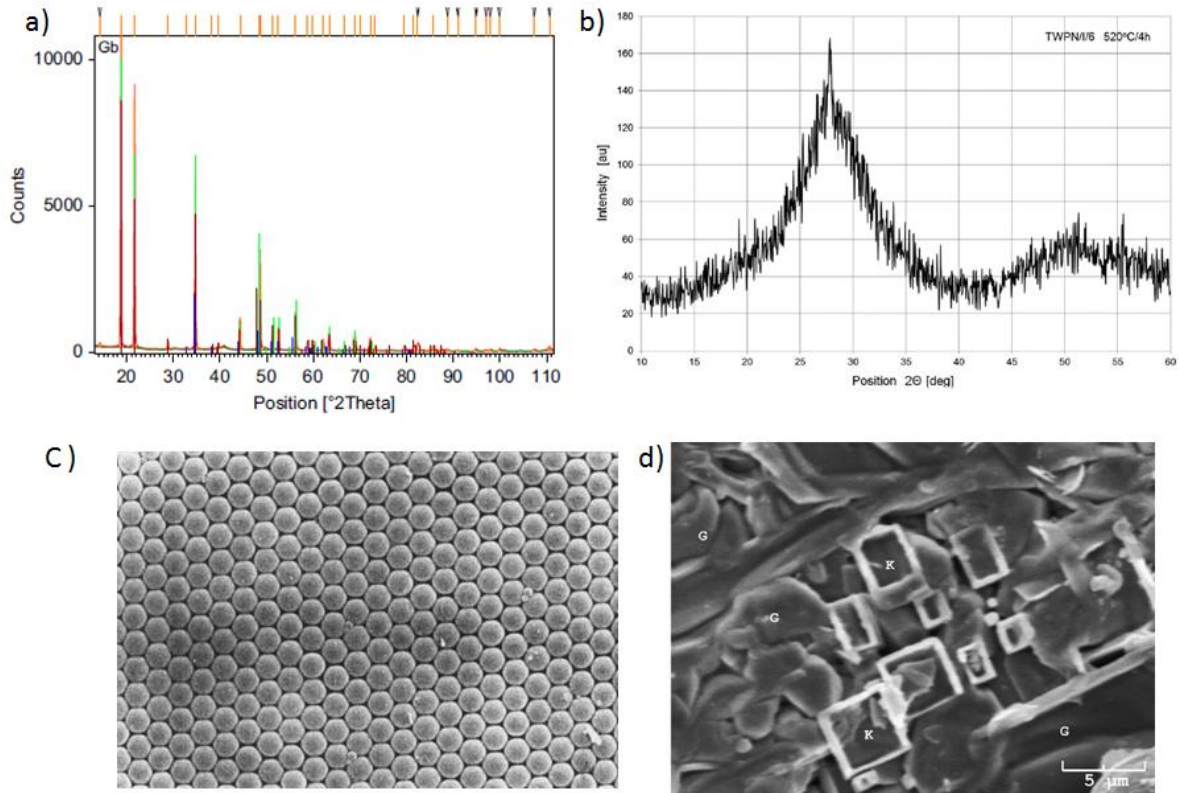
Source: Edited by the author 2012

Why is it important to study the transformation glass to liquid in this temperature range? The glass transition temperature (T_g) determines its mechanical, optical and viscoelastic properties. It should be remembered that glasses, to be a material in a metastable state, tend to reach a steady state, provided it is a permissible temperature. This process is known as structural relaxation.

In conclusion: A glass is any body with amorphous atomic structure, and a crystal is a body with ordered structure.

Figure 1.2 illustrates a didactic form of these differences, there is illustrated the structure of an amorphous glass and the ordered structure of a crystal. It also illustrates the diffractograms characteristic of a glass and crystal.

Figure 1.2. a) Diffraction patterns from a crystal⁷, b) diffraction patterns of a glass⁸, c) SEM micrographs for a crystal⁹ and d) glass¹⁰.



Fountain. Edited by the author 2012

1.2 Host glass.

The chemical composition plays an important role in the development of photonic devices, however, we can mention some limitations:¹¹

- The range of transparency is very important because it excludes important regions that may be useful. For example, mid-infrared lasers cannot be realized with silicate fibers, which are strongly absorbing for wavelengths above 2 μm.

- The glass composition strongly influences the maximum concentration of dopant ions that can be incorporated without excessive clustering, which would result in quenching effects and possibly increased propagation losses;
- Mainly the maximum phonon energy of the host glass determines the rate of multiphonon emission processes, thus the speed of non-radiative transfers between certain levels. This effect can be strong: certain levels may be long-lived (multiple milliseconds) in heavy-metal fluoride glasses, but very short-lived (few microseconds) in silicate glasses;
- Some glasses, for example, fluoroindates, tend to be difficult and expensive to fabricate and handle. Clean fiber cleaves are not always easy to obtain, and often require modified methods;
- Various glasses exhibit high hygroscopicity, strongly affecting their optical and mechanical properties, and so causing instability of the glass;
- A significant parameter is the characteristic temperature T_g . If this temperature is relatively low, we obtain materials sensitive to thermal shocks; etc.

Nevertheless, the above limitations, systematic studies have allowed the development of a variety of glass with optimum optical and chemical properties for the technological development of optoelectronic devices.

1.3 Photonic glasses and crystal.

The optical, chemical, and thermal properties of glasses and crystals have been studied for many decades due to their applications in solid state devices. Following, we present some types of glasses and crystals emerging from systematic studies, and detail some of its properties to technological applications

1.3.1 Silica glasses

When we refer to glassy systems, immediately arise those that are based on silica (SiO_2)¹², and this occurs probably due to its natural origin and its abundance in nature. Besides being the precursor of older glassy systems and having enormous potential for applications¹³, it has always occupied an important place in the glass industry, including more advanced applications such as in telecommunications through optical fibers.

These glasses could be optically transparent from the ultraviolet to the mid-infrared, its attenuation is about 0.2 dB/km at wavelengths of 1550 nm and 0.35 dB/Km at 1300 nm . Another important fact to note is its relatively high phonon frequency around 1100 cm^{-1} .

With these antecedents of limitations, we need to find new vitreous compositions to replacement.

1.3.2 Phosphate glasses

Phosphate glasses are attractive host materials for a variety of photonic devices such as high power lasers, fiber and waveguides amplifiers, optical insulators and other application¹⁴.

These glasses have high transparency, reason by which is important in the UV region. This region is important for a variety of studies, especially the 4f-5d transitions of lanthanide ions. These transitions are used in faraday rotators, photostimulable phosphors for x- ray dosimeters, and gratings imprinted by laser exposure.

Another benefit of high UV transmission is the low damage by laser, which in turn is the precondition for the design of core-cladding devices where the photosensitivity is confined to the core such as in fiber bragg gratings.

Phosphates glasses have low refractive index in range of 1.4 to 1.7, matching to standard telecom fibers. Otherwise, they give rise to high fluorescence lifetimes of RE laser ions, resulting in high gain for lasers and amplifiers.

Compared with silicate glasses, phosphate glasses have low temperatures and viscosities, resulting in convenient process temperatures for device fabrication such as rotational casting, extrusion, fiber drawing....

The local structure of the glasses affects the laser properties of the RE ions. In dependence of the composition, they are attractive host for different laser and amplifier applications.

1.3.3 Low silica calcium aluminosilicate glass

In 1909, Shepherd and colleagues collected small amounts of glass during studies of the ternary system $MgO - CaO - AlO_3$ ¹⁵. Aluminates glass studies emerged after many years later, when investigators found that adding small amounts of SiO_2 increased the glass stability, thus obtaining a high thermal stability parameter, and so obtaining large amounts size of glass. One of the major disadvantages of these glasses is the strong absorption band between 2.7 and 3.8 μm ¹⁶ due to sense the presence of hydroxyl.

1.3.4 Lead indium phosphate

Lead Indium Phosphate glasses have a transparency which makes them useful in the window of visible and infrared electromagnetic spectrum because its transmission window is in the range of 300 to 2800 nm¹⁷.

It is also important to note that these glasses have a relatively high refractive index, (1.7 to 1.9), moderate dispersion (Abbe number of about 30), a high thermal expansion coefficient (10 to $12 \times 10^{-6}/C$)¹⁸.

These glasses have good chemical and mechanical properties and are resistant to radiation, in photonic are used in the manufacture of optical fiber with high numerical aperture (NA ~ 9)¹⁸.

One advantage of these glasses is their low viscosity and low melt temperatures (800 ° C), and it is also a good host to be doped with rare earth ions, having a clear example of the laser Pm³⁺.

1.3.5 Borates glasses

Glasses based on oxides are attractive for obtaining efficient luminescence in trivalent lanthanide ions.

In the case of borate glasses, they are optically good with high transparency, low melting point, a relative high thermal stability and a good capacity to be doped with high concentrations of rare earth ions¹⁹.

However, due to its high phonon frequency ($\sim 1400 \text{ cm}^{-1}$), high efficiency is difficult in the infrared and upconversion processes based on Er³⁺, Tm³⁺ and Ho³⁺ ions.¹⁹

On the other hand, the high phonon energy in these glasses not affects emissions for the ions Sm³⁺ and Eu³⁺, and sometimes it can accelerate the relaxation processes, being necessary and beneficial for emission in the visible²⁰.

1.3.6 Fluoroindate glasses

I. Poulain and colleagues, in 1980, found that the InF mixed with other divalent fluorides generated a new glass, the fluoroindatos²¹. These glasses are emerging as an important family, because they exhibit a higher transmission window (around 10,000 nm), a low phonon frequency ($\sim 510 \text{ cm}^{-1}$), an attenuation of 0.001 dB/km, and better chemical properties and physical than their predecessors, the ZBLAN glass²². These glasses have potential applications in optoelectronic devices and telecommunications. Recently much attention has been given to optical amplifiers at 1.3 μm , for which, Pr^{+3} doped fluoroindates glasses offer promising results.²³

1.3.7 Neodymium-doped yttrium aluminum garnet, Nd:YAG crystal

The YAG (yttrium aluminum garnet) host is a stable system compound, physically hard, optically transparent from below 300 nm to beyond 4 μm . YAG single crystals are good hosts for rare earth ions²⁴.

In the development of modern optics, **the solid-state laser is a very important.** One of the most common lasers is the Nd:YAG (neodymium-doped yttrium aluminum garnet, $\text{Nd:Y}_3\text{Al}_5\text{O}_{12}$).

Nd:YAG laser was initially reported by Bell Laboratories in 1964²⁵, but did not become a tool widely accepted until the 1970s of last century, its first major application was the rangefinder arena. After that, it was gaining acceptance within the military community, scientific, industrial, and medical markets.

Nd YAG laser can be used in continuous or pulsed mode. Its most important emission is at 1064 nm²⁶, however, 1.3 and $\sim 0.9 \mu\text{m}$ have also been well exploited. Another important application is in nonlinear optics, where it can be easily used to create double frequency output laser at 532 nm and several other nonlinear processes which covers regions of UV and IR²⁶. The Figure 1.3 shows the energy levels of the Nd:YAG laser.

1.3.8 Yttrium Vanadate (YVO₄) crystal

The Yttrium orthovanadate (YVO₄) is a positive uniaxial crystal. It has excellent optical properties and thermal stability wide. It is ideal for optical polarizing components because of its wide transparency (~ 0.4 to 5 μm) and large birefringence (0.2039 at 1550 nm)²⁷.

The Nd:YVO₄ has large stimulated emission cross-sections at both 1064 nm and 1342 nm. Although the lifetime of Nd:YVO₄ is about 2.7 times shorter than that of Nd:YAG²⁹, the stimulated emission cross-section of an a-axis cut Nd:YVO₄ at 1064nm is about 4 times higher than that of the Nd:YAG²⁸.

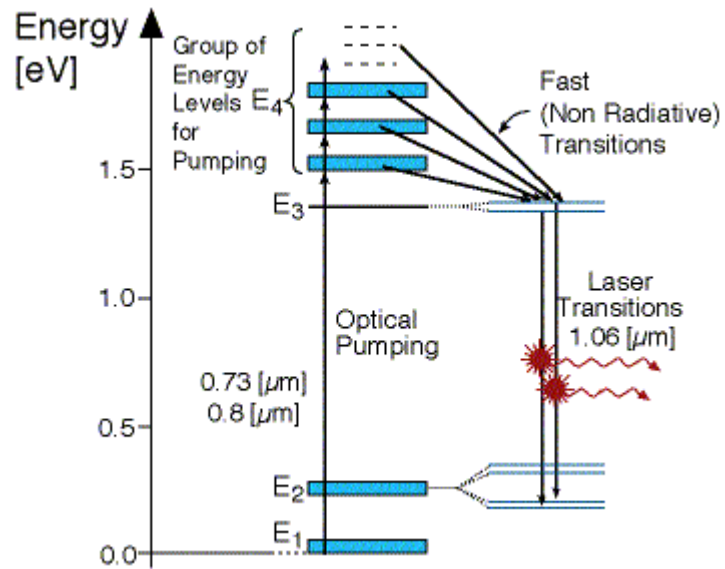
1.3.9 Gadolinium Orthovanadate (GdVO₄) crystal.

Neodymium doped Gadolinium Orthovanadate single crystal (Nd:GdVO₄ crystal) was first introduced as a laser material in 1992 by Zagumennyi *et al.*³⁰ This is an excellent laser crystal, presenting good physical, optical, and mechanical properties. It has higher slope efficiency than Nd:YAG and better thermal conductivity.

Many other glasses and crystals have been studied in order to optimize their properties. The literature has reported studies of many glassy matrices and crystals that have good physical and chemical characteristics, and they can be doped with sufficient quantities of rare earths.

Different research groups investigate these types of materials and are intended to improve existing applications and develop new devices for technological interests.

Figure 1.3. Energy level diagram of a Nd:YAG laser



Source: <http://perg.phys.ksu.edu/vqm/laserweb/ch-6/f6s2t2p2.htm>

2 SPECTROSCOPIC PROPERTIES OF SOLIDS

2.1 Introduction to spectroscopic models

In the nineteenth century, with the discovery of dark lines in the solar spectrum and the emission lines of flames, arcs and sparks, spectroscopy was considered as a necessary tool for the realization of chemical and physical analyses. In the mid-nineteenth century was seen the absorption and emission spectra of hydrogen atom, which consist of lines or narrow bands of characteristic frequencies. By this time, the experimental problem was to correlate the various lines and bands observed in the spectra with the chemical nature of the substance that emits, problem that was not easy to solve, even after the rise of quantum mechanics. But, nowadays we find all the spectral characteristic of the elements that exist in nature.

The first line was found by Balmer in 1885, and an empirical equation to explain the spatial arrangement between the lines of the emission spectrum of hydrogen atom is³¹:

$$v = R \left(\frac{1}{2^2} - \frac{1}{n^2} \right) \quad (2.1)$$

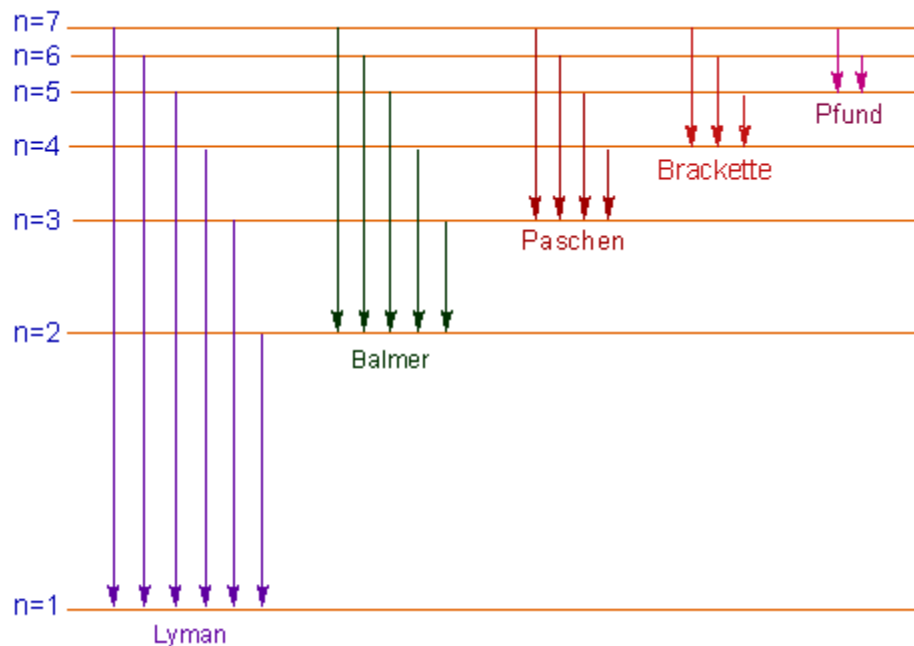
Where v is the wave number of a particular line, R is the Rydberg constant and $n = 3, 4, 5...$

Later similar series were found to more complex atoms. These series are identified by their discoverer. In Table 2.1 and figure 2.1 show the different series.

Table 2.1. Spectral series

Spectral series	Spectral region	n_1	n_2
1. Lyman series	Ultra-violet	1	2, 3, 4, ...
2. Balmer series	Visible	2	3, 4, 5, ...
3. Paschen series	Near infra-red	3	4, 5, 6, ...
4. Brackett series	Infra-red	4	5, 6, 7, ...
5. Pfund series	Far infra-red	5	6, 7, 8, ...

Source: Author 2012.

Figure 2.1. Transitions of spectral series.

Source: <http://www.adichemistry.com/>

After the development of quantum mechanics, the quantitative development of spectroscopic data was possible and, in fact, atomic spectroscopy was the first experimental evidence provided, from which were derived the various postulates of quantum mechanics.

In the year 1900, Max Planck, in his study of black body radiation, found that the laws of radiation could not be explained by purely thermodynamic basis, then Planck hypothesized that the absorption and emission of energy by matter could not be carried continuously, only in "quantum" finite energy, $E = h\nu$, where h is today known as the Planck constant ($h = 6.625 \times 10^{-34} \text{ j.s}$).

With her atomic theory, Bohr's, year 1913, obtained a spectacular achievement for the origin of spectral lines. To explain the fact that the hydrogen atom emits only at certain characteristic frequencies, Bohr postulated that, in atoms, electrons occupy states or levels to certain values of energy (or frequency) well defined. The cause that one atom emits light is that the electron located in a higher energy level E_h , drops to a lower energy state E_l , in a manner that:

$$E_h - E_l = \Delta E = h\nu \quad (2.2)$$

where E_h and E_l are the higher and lower energy levels, respectively. Thus, when a transition occurs electronically, a photon of energy $h\nu$ is emitted. Inversely, the atom can absorb a photon and undergoes a transition to a higher energy state/level. Bohr (1913) developed a theoretical model for the spectrum of hydrogen atom, which could lead to the Rydberg constant, obtaining³²:

$$R = \frac{2\pi^2 m_e e^4}{ch^3} (\text{cm}^{-1}) \quad (2.3)$$

substituting m_e the mass of the electron, e the electric charge, c the speed of light, and h the Planck's constant, by their respective values, the result is of $1.097 \times 10^7 (\text{cm}^{-1})$.

There were other changes to the work on the atomic structure of Bohr. In 1926, Erwin Schrodinger, incorporating the wave and particle properties of electromagnetic radiation and the Heisenberg uncertainty principle, developed the theoretical form of quantum mechanics as we know so far to describe the behavior of microscopic systems. Since then, there have been many theoretical developments in order to find the solution of the Schrödinger equation applied to various particular systems. For example, the Schrödinger equation independent of time, applied to the hydrogen atom is given by:

$$\nabla^2\Psi + \frac{2m}{\hbar^2}(E + V)\Psi = 0 \quad (2.4)$$

where m is the mass of the electron $V = -e^2/r$ is the potential energy due to electrostatic interaction and r is the distance between the electron and the core. Ψ is the wave function, which describes the probability that an electron will be found in a certain state. Usually it is convenient to express the wavefunction Ψ in polar coordinates, because it can be expressed mathematically as a product of the radial R and the angular Y parts, thus:

$$\Psi = R(r)Y_{l,m}(\theta, \phi) \text{ or also } \Psi(r, \theta, \phi) = R(r)\Theta(\theta)\Phi(\phi) \quad (2.5)$$

So the Schrödinger equation in polar coordinates is:

$$\frac{\partial^2\Psi}{\partial r^2} + \frac{2}{r} \frac{\partial\Psi}{\partial r} + \frac{1}{r^2\sin\theta} \frac{\partial(\sin\theta \left(\frac{\partial\Psi}{\partial\theta}\right))}{\partial\theta} + \frac{1}{r^2\sin\phi} \frac{\partial^2\Psi}{\partial\phi^2} + \frac{2m}{\hbar^2}(E + V)\Psi = 0 \quad (2.6)$$

This expression is the differential equation of the wave function for the electron in a hydrogen atom, which, under certain conditions, completely specifies the behavior of the electron. Development for the solution of this equation is found in various books of quantum mechanics or the atomic structure theory,^{33,34} and this is not the case mentioned here. What is important to mention here is that solving Eq (2.6) is required four quantum numbers, including spin to describe the electron in a hydrogen atom. For the nomenclature used in this field, it sufficient to consider the four fundamental

quantum numbers usually described by n, l, m_l, m_s and these are: the principal quantum number, azimuthal, magnetic, and spin. The principal quantum number n , as its name implies, is the main energy index for an electron and it takes all integer values from the unity to infinity (in which case, the electron is removed from the atom, leaving it ionized). For other quantum numbers are:

$$l = 0, 1, 2 \dots \dots n - 1$$

$$m_l = -l, -l + 1, \dots \dots 0, \dots \dots +l$$

$$m_s = \pm \frac{1}{2}$$

And those electrons with $l = 0, 1, 2, 3, 4$ are known by the letters s, p, d, f, g , respectively. In this scheme the ground state configuration of the electrons is characterized by a coefficient that identifies the layer or energy level, a letter that identifies a sub-level and a superscript that identifies the number of electrons in the layer or sublayer.

When more than one electron has to be considered, the atomic quantum numbers are defined by:

$$L = \sum l_i \quad M_l = \sum (m_l)_i \quad S = \sum m_s$$

and the multiplicity of the spin: $m = 2S + 1$

where L represents the total magnetic moment (with $L = 0, 1, 2, 3, 4, \dots$) and are represented by the letters S, P, D, F, G, \dots respectively). J is a vector specifying the direction that keeps the total angular momentum and spin angular momentum and is given by $J = S + L$.³⁵

2.2 General considerations of the optical properties of rare earth ions

We mentioned earlier that the hydrogen atom is the simplest example of an atomic system. When Erwin Schrödinger got his famous equation, the first problem faced and successfully solved was the determination of the structure of the hydrogen atom. These results provided convincing evidence that the new theory was correct.

The importance of the hydrogen atom is the fact of it to be based on two important considerations: First - the eigenvalues obtained for the energy are consistent with experimental results and, therefore, are illustrative; Second - many of the results obtained for the hydrogen atom are more general than the Coulomb potential, which is used for determining and hold for any central force field, i.e., for any radial force directed toward the center of attraction that depends only on distance, not on the angle. This is very important because when approaching the problem of many electrons atoms (as is the case of rare earth ions) to a central field, which, however, differs from an inverse square field, some the results obtained for the hydrogen atom can be used. The relevant characteristic that allows this generalization is based on a central field not producing torsion moment on the particle and, therefore, from classical mechanics, it is known that the angular momentum is maintained constant, and this resulted has a counterpart in the wave mechanics, which consequently leads to the quantization of the angular momentum.

Another important point is that the Schroedinger equation can be solved not only so accurate for the hydrogen atom, but also for hydrogen-like atoms:

$He^+, Li_e^+, Be_{ee}^{3+} \dots$, and simple molecular ion compounds by a single electron.³⁶ Despite the complicated mathematics, the hydrogen atom is a simple mathematical problem, however, any atom or ion that has more than one electron is so complicated that an exact solution of the problem is impossible.

In the case of the helium atom, approximate solutions have been developed with good results compared with experiments. However, the methods used for the helium

atom are quite complicated to be applied to atoms with more than two electrons, and so it is preferred to use some simple approximations to simplify the study of atoms or ions with many electrons.

Below is a brief summary of the main ideas of an approximation method that is regularly used in the study of atoms or ions with many electrons (as in the case of rare earth ions).

The Hartree method³⁷ is extremely useful in solving the time-independent Schrödinger equation to a system of Z electrons moving independently in the atom. The equation can be separated into a set of Z equations of Schrödinger independent of time, all in the same manner, each of which describes an electron moving independently in a net potential. One of these time-independent equations for an electron is given by:

$$\left[\frac{-\hbar^2}{2m} \nabla^2 + V(r) \right] \Psi(r, \theta, \phi) = E \Psi(r, \theta, \phi) \quad (2.7)$$

where r, θ, ϕ are the polar coordinates for an electron, ∇^2 is the Laplacian operator, E is the total energy of the electron, $V(r)$ is the net potential, and $\Psi(r, \theta, \phi)$ is the eigenfunction of the Hamiltonian. The total energy of the atom is the sum of Z total energies E . The eigenfunction associated with the atom is obtained by multiplying the Z eigenfunctions that describe electrons moving independently. The problem is that to begin the process the expression for the net potential $V(r)$ experienced by an electron is not known and, therefore, it should be determined by means of a self-consistency treatment complying with the following requirements:

- A. First, made a reasonable assumption of the form that must satisfy the potential $V(r)$ for boundary values:

$$V(r) = \begin{cases} -\frac{ze^2}{r}, & r \rightarrow 0 \\ -\frac{e^2}{r}, & r \rightarrow \infty \end{cases}$$

Below is to make a reasonable interpolation for intermediate values of r . This can be done if one remembers that an electron very near to the nucleus experiences a Coulomb attraction due to nuclear charge $+Ze$, whereas for an electron very far to the core experiences the power of a charge $+e$ due to the shielding of nuclear charge by the charge $-(Z - 1)$ of the rest of the electrons around the nucleus.

- B. Time-independent Schrödinger's equation for a representative electron is solved for the potential $V(r)$ that was proposed in the previous step. This is not an easy task because the radial part of the equation must be resolved by numerical integration. Representative eigenfunctions obtained for an electron are of the form: $\Psi_\alpha(r, \theta, \phi)$, $\Psi_\beta(r, \theta, \phi)$, $\Psi_\gamma(r, \theta, \phi)$, ..., each of the symbols $\alpha, \beta, \gamma, \dots$, refers to a full set of three numbers space and one for each electron's spin.
- C. To determine the atom's ground state, the quantum states of the electrons are filled in such a manner that minimizes the total energy and satisfies the condition of the Pauli's exclusion principle, i.e., the states are filled in order of increasing energy, with one electron in each state. Thus the eigenfunction for the first electron is $\Psi_\alpha(r_1, \theta_1, \phi_1)$; the eigenfunction for the second is $\Psi_\alpha(r_2, \theta_2, \phi_2)$; and so on for the Z eigenfunctions corresponding to Z eigenvalues of lower one obtained in the previous step.
- D. Evaluate the atom's charge distributions from the eigenfunctions obtained in the previous step. This is done by taking the charge distribution for each electron as the product of its charge $-e$ multiplied by the probability density function $\Psi^*\Psi$. The justification is that $\Psi^*\Psi$ determines the probability that the charge lies on different positions in the atom. The charge distributions of the $(Z - 1)$ representative electrons are added to the distribution of nuclear charge $+e$ at the origin to determine the distribution of total charge in the atom such as perceived by one representative electron.

- E. Using Gauss's law to determine the electric field which is produced due to the distribution of the total charge obtained in the previous step. Evaluate the integral of this electric field to obtain a precise estimate of net potential experienced by a representative electron. The new obtained potential $V(r)$ generally differs of the proposed value in step A.
- F. If the potential is significantly different, the procedure is repeated, starting at step B using for this purpose the new $V(r)$. After several cycles, the obtained potential at the end is essentially the same as that used initially. This net potential is self-consistent and the eigenfunctions calculated for this potential describe the electrons in the ground state of the atom.

In the Hartree method there are two important conditions that must be satisfied: the weak and the strong. The weak condition refers to the Pauli's exclusion principle which is satisfied for step three, that only one electron populates each quantum state.

The strong condition refers to the condition of asymmetry. If the strong condition is not satisfied, it does not use completely asymmetric eigenfunctions. The reason is that an antisymmetric function would involve a linear combination of terms $Z! = Z(Z - 1)(Z - 2) \dots 1$, which is an extremely large number for all atoms, except for those with small Z values.

The principal effect of using totally antisymmetric functions is to reduce the spacing between certain pairs of electrons, and increase the separation between others. This leaves the average charge distribution of the atom essentially unchanged. Since average charge distribution is important in the Hartree method, using eigenfunctions that not exhibit a definite asymmetry not introduce significant error. This was subsequently verified by Fock.³⁸ However, the asymmetric functions are totally necessary to describe atoms of many electrons in excited states. The results obtained in Hartree approximation provide a quite satisfactory explanation of the essential characteristics of atoms of many-electron in their ground states.

2.3 Optical properties of free ions

The rare earths are characterized by the progressive filling of the $4f$ or $5f$ - shells of their electronic configuration. They occur as two groups, each with fourteen elements, known as the lanthanides and the actinides.

The lanthanides, the object of our study, are associated with the progressive filling of the $4f$ shell, beginning with the element cerium ($Z = 58$) and finishing with the lutetium ($Z = 71$). All them have the same electronic configurations $5s^2 5p^6 6s^2$, but incomplete $4f$ shell, being filled progressively. The oxidation state prevailing in the lanthanides is +3. This is the most common form of incorporation of lanthanide ions in glasses and crystals. Table 2.2 shows some important characteristics of lanthanide ions. It is important to mention that the rare earths have the most complicated spectra of all elements of the periodic table.

Table. 2.2. Characteristics of lanthanide ions

Z	Element	Atomic Configuration	Atomic Ground State	Configuration X^{3+}	Ground State X^{3+}	Radius X^{3+} Å
57	La	$4f^0 5d^1 6s^2$	$^2D_{3/2}$	$4f^0$	1S_0	1.061
58	Ce	$4f^1 5d^1 6s^2$	1G_4	$4f^1$	$^2F_{5/2}$	1.034
59	Pr	$4f^2 5d^1 6s^2$	$^4I_{9/2}$	$4f^2$	3H_4	1.013
60	Nd	$4f^3 5d^1 6s^2$	5I_4	$4f^3$	$^4I_{9/2}$	0.995
61	Pm	$4f^4 5d^1 6s^2$	$^6H_{5/2}$	$4f^4$	5I_4	0.979
62	Sm	$4f^5 5d^1 6s^2$	7F_0	$4f^5$	$^6H_{5/2}$	0.964
63	Eu	$4f^6 5d^1 6s^2$	$^8S_{7/2}$	$4f^6$	7F_0	0.950
64	Gd	$4f^7 5d^1 6s^2$	9D_2	$4f^7$	$^8S_{7/2}$	0.938
65	Tb	$4f^8 5d^1 6s^2$	$^6H_{15/2}$	$4f^8$	7F_6	0.923
66	Dy	$4f^9 5d^1 6s^2$	5I_8	$4f^9$	$^6H_{15/2}$	0.908
67	Ho	$4f^{10} 5d^1 6s^2$	$^4I_{15/2}$	$4f^{10}$	5I_8	0.894
68	Er	$4f^{11} 5d^1 6s^2$	3H_6	$4f^{11}$	$^4I_{15/2}$	0.881
69	Tm	$4f^{12} 5d^1 6s^2$	$^2F_{7/2}$	$4f^{12}$	3H_6	0.869
70	Yb	$4f^{13} 5d^1 6s^2$	1S_0	$4f^{13}$	$^2F_{7/2}$	0.858
71	Lu	$4f^{14} 5d^1 6s^2$	$^2D_{3/2}$	$4f^{14}$	1S_0	0.848

Source: Lanthanide and Actinide Chemistry. John Wiley & Sons

For several decades, it is known that the spatial extent of the $4f$ eigenfunction rapidly begins to contract at the beginning of the lanthanide series.³⁹ The eigenfunction

$4f$ of lanthanum even extends to the edge of the closed $5s^25p^6$ shells, but for neodymium, its eigenfunction has contracted sufficiently, such that its maximum is found within the $5s^25p^6$ shells. The contraction of the eigenfunction f in the rare earths is reflected in some of its properties. Due to this contraction, the active shell behaves like an inner shell. This absence of extension of the eigenfunction f in the environment of the ion, together with the electron shielding by the $5s^25p^6$ shell, generally do not allow the submission of any strong interaction of electrons with their ligand. The effect of the contraction of the eigenfunction f is also evident in the regular decrease the size of the lanthanide ions as atomic number increases. $4f$ electrons have orbital radii that go from 0.6 \AA for the case cerium to 0.35 \AA for the lutetium. The shield of the $4f$ electrons, experienced by the $5s^2$ shell, is one of the most important characteristics of the rare earth ions, which makes a species of "quasi-atoms", such that the ion energy levels will not be significantly affected when the ion is introduced into a crystal or glass.

2.4 ENERGY LEVELS

According to wave mechanics an electron is described by its wave function. The energy values are given by the eigenvalues of the equation:

$$H\Psi = E\Psi \quad (2.8)$$

The solution for atoms or ions with one-electron is not a problem. In these cases, the Hamiltonian H contains only the terms corresponding to the kinetic energy and the energy of electrostatic attraction between the nucleus and the electron. Thus, the values for the energy of atom or ion can be calculated accurately. This is not the case for multielectron atoms (such as trivalent ions of rare earths). In this case, the Hamiltonian contains an additional term, which takes into account the electrostatic repulsion between electrons. Due to this term in the Hamiltonian, the exact calculation of E in equation (2.8) becomes very complicated. Therefore, it has become common practice to use several approaches to simplify the problem being, thus, not possible to find an exact solution for the values of the energy of electrons in multi-electronic atoms. The following, we will

address the problem of how to determine the energy levels of a multi-electronic ion or atom.

The Hamiltonian for a nonrelativistic free ion to an atom of N electrons and nuclear charge $+Ze$ is given by:⁴⁰

$$H = -\frac{\hbar^2}{2m} \sum_{i=1}^N \nabla_i^2 - \sum_{i=1}^N \frac{Ze^2}{r_i} + \sum_{i<j}^N \frac{e^2}{r_{ij}} + \sum_I \lambda_i \vec{l} \cdot \vec{S}_{ij} \quad (2.9)$$

where we have assumed that the core mass is "infinite". The first term of equation (2.9) represents the sum of the kinetic energies of all electrons. The second term represents the Coulomb interaction between each electron and the positive nucleus at the distance r_i , i.e., represents the Coulomb potential energy of all the electrons in the core electric field. The third term represents the Coulomb potential energy of the interactions (repulsive) between pairs of electrons found in the relative distance r_{ij} . The fourth term represents the spin-orbit interaction. The later interaction is responsible for the fine structure of the spectrum. It will be analyzed then, the impact on energy levels of the atom (or ion) of each term of the Hamiltonian for a free ion (2.9).

The non existence of exact solutions to Schrödinger equation of atomic systems with more than one electron makes necessary the introduction of some approximations. These approximations result in the solution of Schrödinger equation in different schemes. If you only consider the first and third terms of (2.9), we have the following expression:

$$H = -\frac{\hbar^2}{2m} \sum_{i=1}^N \nabla_i^2 + \sum_{i<j}^N \frac{e^2}{r_{ij}} \quad (2.10)$$

This Hamiltonian can be rewritten in a more general form, in such way that it represents a system of N charged particles that interact in a binary manner, as:

$$H = -\hbar^2 \sum_{i=1}^N \frac{\nabla_i^2}{2m_i} + \sum_{i<j}^N V(r_{ij}) \quad (2.11)$$

One of the most widely used methods to solve the equation (2.8) with the Hamiltonian (2.11) in a first approximation is referred to "Independent Particle Model", which basically consists in considering that each particle of the system moves in a common potential $U = \sum U_i(r_i)$ due to the interaction of the particle with the rest of the particles. With this in mind, the earlier Hamiltonian can be rewritten using U as:

$$H = \frac{-\hbar^2}{2} \sum_{i=1}^N \frac{\nabla_i^2}{m_i} + \sum_{i=1}^N V_i(r_i) + \left[\sum_{i<j}^N V(r_{ij}) - \sum_{i=1}^N U_i(r_i) \right] \quad (2.12)$$

Now everything is reduced to determine U in a manner that approximates the real potential as possible. Therefore, it must satisfy the following:

$$\left| \left[\sum_{i<j}^N V(r_{ij}) - \sum_{i=1}^N U_i(r_i) \right] \right| \rightarrow 0 \quad (2.13)$$

The value of U can be obtained via self-consistency of the eigenfunctions obtained with the first two terms of (2.12):

$$H_i^{(0)} \Psi_i^0 = E_i \Psi_i^0; i = 1, 2, \dots, N \quad (2.14)$$

where:

$$H_i^{(0)} = -\frac{\hbar^2}{2} \frac{\nabla_i^2}{m_i} + U_i(r_i) \quad (2.15)$$

and

$$U_i(r_i) = \int V(r_{ij}) \Psi_j^{(0)*}(r_i) \Psi_j^{(0)}(r_j) d\tau_j \quad (2.16)$$

Now, one applies the self-consistency condition proposing a test function for each of the equations (2.14), and with the help of these functions, the U_i value is evaluated by the equation (2.16). The value obtained for the function U_i is again applied in equation (2.14) to determine a new function $\Psi_i^{(0)}$. The method is repeated until obtaining the

same function product as the previous, moment in which the self-consistency is obtained and with it an optimum value for U_i . The method should be repeated for each of the N particles, such that in the end of the process the wave function representing the system can be written as:

$$\Psi^{(0)}(r_i) = \Psi_1^{(0)}(r_1) + \Psi_2^{(0)}(r_2) + \dots + \Psi_N^{(0)}(r_N) \quad (2.17)$$

While the energy of the system is obtained by:

$$E = E_1 + E_2 + \dots + E_N \quad (2.18)$$

With this, the Hamiltonian (2.11) can be written as:

$$H = -\frac{\hbar^2}{2} \sum_i^N \frac{\nabla_i^2}{m_j} + \sum_{i<j}^N U(r_i) \quad (2.19)$$

that is a general expression.

Applying the previous expression to a multi-electronic atom or ion, we have:

$$H_{cc} = \left[-\sum_i^N \frac{\hbar^2}{m_i} \nabla_i^2 + U(r_i) \right] \quad (2.20)$$

The difference between the expression (2.9) (without the fourth term) and (2.20) can be considered as a potential perturbation:

$$H - H_{cc} = V = \sum_i^N \left[-\frac{Ze^2}{r_i} - U(r_i) \right] + \sum_{i<j}^N \frac{e^2}{r_{ij}} \quad (2.21)$$

The corresponding Schrödinger equation that needs to be solved for the Central field approximation is given by:

$$\sum_{i=1}^N \left[-\frac{\hbar^2}{2m} \nabla_i^2 + U(r_i) \right] \Psi = E_{cc} \Psi \quad (2.22)$$

which can be separated if you choose a solution such as:

$$\Psi = \sum_{i=1}^N \varphi_i(a^i) \quad \text{and} \quad E_{cc} = \sum_{i=1}^N E_i \quad (2.23)$$

Each electron moving in the central field $U(r_i)$ must satisfy equations that have the following form:

$$\left[-\frac{\hbar^2}{2m} \nabla^2 + U(r) \right] \varphi(a^i) = E_{cc}(a^i) \varphi(a^i) \quad (2.24)$$

where (a^i) represents a set of quantum numbers (nlm) that specify the state of motion of each electron in the central field.

You can make an additional separation of variables if introduced polar coordinates (θ, ϕ, r) and separate the eigenfunctions for an electron in angular and radial parts. The normalized solution resulting for bound states can be written as:

$$\varphi(a^i) = R_{nl}(r) Y_{lm_l}(\theta, \Phi) / r^{-1} \quad (2.25)$$

The radial function R_{nl} depends on the potential energy function $U(r)$ of a center field. While the spherical harmonics are defined by:⁴¹

$$Y_{lm}(\theta, \Phi) = (-1)^m \left[\frac{(2l+1)(l-|m|)!}{4\pi(l+|m|)!} \right]^{1/2} P_l^m(\cos \theta) e^{im\Phi} \quad (2.26)$$

with,

$$P_l^m = \frac{(1-w^2)}{2^l l!} \frac{d^{m+1}}{dw^{m+1}} (w^2 - 1)^l. \quad (2.27)$$

Now, the solutions of the equation (2.22), with due inclusion of spin can be written as:

$$\Psi = \sum_i^N \varphi(\alpha^i), \quad (2.28)$$

where α_i represents the quantum numbers (n, l, m_l, m_s) of the i th electron. However, this solution is not unique since other solutions can be obtained if the coordinates of any of the N electrons are permuted. Thus, to comply, with the Pauli's exclusion principle,

$$H = - \sum_{i < j}^N \frac{e^2}{r_{ij}} \quad (2.32)$$

solving the following determinant:

$$\left| \left(\varphi(ai) \left| - \sum_{i < j}^N \frac{e^2}{r_{ij}} \right| \varphi(a^j) \right) - \Delta E \delta(i, j) = 0. \right| \quad (2.33)$$

This determinant of degree n in the general case contains n roots ΔE_i , correspond to corrections to energy. The Hamiltonian in the approximation of Russell-Saunders commutes with L^2, S^2, J^2 and with the component z of angular numbers L_z, S_z , and J_z . The quantum numbers L, S, J, M_j, M_s, M_l are good quantum numbers to describe the (RS) states. However, as only four are independent, usually is select the set $(SLJM_j)$.

The energy levels do not depend on M_s and M_l , so the representation $(SLM_l M_s)$ can be changed by $E(S, L)$. Additionally, as the states $(SLJM_j)$ can be represented as linear combinations of states $(SLM_l M_s)$, energy levels do not depend on J and M_j . Therefore, in the scheme of Russell-Saunders, the energy levels, called multiplets, can be represented by ^{2s+1}L . In the Russell-Saunders approximation, the fourth term of equation (2.9), namely the spin-orbit interaction, is considered as a small perturbation to the states. Using perturbation theory independent of time, the corrections to energy levels are made, which are given by:

$$\Delta E = \left\langle SLJM_j \left| \sum_i \lambda \vec{l}_i \cdot \vec{s}_i \right| S'L'J'M'_j \right\rangle = \frac{1}{2} \zeta(SL) [J(J+1) - L(L+1) - S(S+1)] \quad (2.34)$$

That gives rise to the rule of Lande and splits terms ^{2s+1}L in their corresponding components $^{2s+1}L_j$. This perturbation gives origin to a weak splitting at the levels associated with SL , and so it is known as fine splitting or fine structure.

So far we have, for a first order approximation, the energy levels identified by its corresponding configuration $(n_1, l_1)(n_2, l_2) \dots (n_N, l_n)$. In other words, the electrostatic interaction between electrons splits the levels of the configuration in different components (SL). Adding the spin-orbital interaction breaks weakly the degenerescence in J , leading to the representation of the terms $^{2S+1}L_J$. Now well, as J can have all values between $L + S$ and $L - S$, for a total of $2S + 1$ components, then $2S + 1$ expresses the multiplicity or number of lines of the multiplet; so, if $2S + 1 = 1$, the term is called singlet, if $2S + 1 = 2$, doublet, etc.

Another important approximation is known as the intermediate coupling approximation, which is very useful for the case of heavy atoms or ions, where the electrostatic interaction is approximately in the same order that the spin-orbit interaction. For this case the Hamiltonian [expression (2.9)] should be considered in complete form, that is:

$$= -\frac{\hbar^2}{2m} \sum_{i=1}^N \nabla_i^2 - \sum_{i=1}^N \frac{Ze^2}{r_i} + \sum_{i<j}^N \frac{e^2}{r_{ij}} + \sum_i \lambda_i \vec{l}_i \cdot \vec{s}_i. \quad (2.35)$$

This Hamiltonian commutes with S , L , M_L , M_S , J^2 , and J_z but does not commute with L^2 , S^2 , L_z , and S_z , and this causes J and M_J to remain good quantum numbers but not S , L , M_L , M_S . To make corrections to the Russell-Saunders scheme is necessary to diagonalize simultaneously the electrostatic and spin-orbit contributions in the representation $|SLJM_J\rangle$. This means that it requires solving the equation given by the determinant:

$$\left| \left\langle SLJM_J \left| \sum_{i<j}^N \frac{e^2}{r_{ij}} + \sum_i \lambda_i \vec{l}_i \cdot \vec{s}_i \right| S'L'J'M' \right\rangle - \Delta E(i, j) \right| = 0. \quad (2.36)$$

Now, because the matrix elements (2.36) are different from zero only between states with the same value of J , (J is a good quantum number), the determinant (2.36) can be divided into subdeterminants where each one is associated with a particular value of J . The solution for each J carries a mixture of states SL given by:

$$|[SL]JM_J\rangle = \sum A(SL)|SLJM_J\rangle. \quad (2.37)$$

The result obtained in the intermediate coupling scheme is the rupture of degeneracy in J of the levels SL , and this in turn leads to a rupture of the rule of Lande intervals. In the intermediate coupling scheme, the states are identified by the component SL that presents best contribution in the mixture, denoted inside brackets to express that they are not pure states.

Now, when the different coupling schemes are analyzed in general form, it is time to return to center field solution to calculate the matrix elements for the states of the f_N configuration of rare earth ions. In the central field solution is obtained a set of antisymmetric wave functions of zero order. These functions can be used to calculate the matrix elements of additional perturbations, always obtaining the results in product form integral radial with their respective angular parts. However, the angular parts can be calculated of exact form using tensor methods and group theory, and the radial integrals can be evaluated as a solution of the radial wave equation, or left as experimental parameters to be determined to make the measures of the perturbation, then, is to find an appropriate form of label the states of the ion. For that we must return to the Hamiltonian of the ion.

The calculation of the Hamiltonian matrix elements of the perturbation is much easier if we define a set of states in terms of a coupling scheme known. Usually the approach is such that we consider only the set of states of the particular configuration that is being studied. This leads to not taking into consider the interactions between different configurations, but can sometimes happen that the approximation is not valid. To avoid this difficulty is usually chosen a coupling scheme that fits best to the physical coupling of the configuration under study. In some cases none set of coupling schemes will approach the case of physical coupling of interest. However, even in these cases can still be calculated the matrix elements of the Hamiltonian of perturbation in terms of the basis states of a coupling scheme established, and then perform a transformation for obtaining the coupling scheme of interest. A coupling scheme that is used very frequently is the Russell-Saunders (who was seen earlier). In this scheme adds the orbital angular momentum of electrons to obtain a total angular momentum L , and the

same operation is performed with the spins to obtain an overall spin S . Below L and S are coupled to obtain a total angular momentum. The numbers L and S are said to define one term of the configuration. In those configurations, where it is present more than one term with the same values of L and S , will need to introduce an additional quantum number τ to distinguish properly these terms. Here it should be noted that, to determine an appropriate manner possible, LS terms of a configuration requires consideration only of those electrons which are not found in closed shell, since the net angular momentum of electrons which are in closed shell is always equal to zero. So, in order to properly label a particular ground state configuration is required to specify the quantum numbers $\tau SLJM$, and can be written as $\Psi(\tau SLJM)$. The matrix elements associated with this state may be written as $\langle \tau SLJM | H_p | S'L'J'M \rangle$, where H_p is the term in the Hamiltonian that represents the system accounting for the perturbation. Unfortunately, new problems arise when trying to explain adequately the states in f^N configuration of rare earth ions.

The fundamental problem resides in the fact that frequently occur states that have the same quantum numbers LS and, therefore, must be added additional quantum numbers to allow adequate differentiation of these states recurrent. G. Racah⁴⁴ solved the problem of systematic classification of states for any configuration f^N ingeniously using for this purpose the theory of groups. Racah's method consists in classifying the complete set of states of the f^N configuration according to their properties under certain transformations of groups. The properties of these groups are used to simplify the calculation of the matrix elements of operators corresponding to tensor interaction being studied. You can describe the way that a particular state transforms under the operations of a group if you use the irreducible representations of the group as labels. These irreducible representations then play a role equivalent to the quantum numbers. A fairly detailed study of this method and its application to the f^N configuration was carried out by Judd⁴⁵ and Ofelt⁴⁶.

To calculate the energy levels of a polyelectronic atom or ion, such as rare earth, first, it should work with the matrix elements of the electrostatic potential defined by expression of the perturbation V :

$$V = \sum_i^N \left[-\frac{Ze^2}{r_i} - U(r_i) \right] + \sum_{i<j}^N \frac{e^2}{r_{ij}}. \quad (2.38)$$

The first term is purely radial and contributes to cause the same displacement of the energy levels that belong to the same configuration, without affecting the structure of the levels. In the case of the second term, the things are different because the repulsive Coulomb interaction of electrons, $\sum_{i<j}^N \frac{e^2}{r_{ij}}$, is different for various states of the same configuration. The summation extends over all electrons. This is convenient to remember that the terms of the energies of a configuration that contains shells are the same, except for a constant energy shift, which happens to be the same for all terms. Therefore, when considering the structure of the energy levels of a configuration, one may restrict the summation in equation (2.10) to electrons that are shells partially filled. This means that, to calculate the energy levels structure produced by a configuration of the type Coulomb repulsive interaction, one must calculate the matrix elements that have the following face:

$$\left\langle SLJM \left| \sum_{i<j} \frac{e}{r_{ij}} \right| \tau' S' L' J' M' \right\rangle. \quad (2.39)$$

Given that the electrostatic Hamiltonian commutes with angular momentum operators associated with L^2, S^2, J , and M , the matrix elements will be diagonal in L and S (but not τ), and independent of J and M . The calculation of matrix elements (2.39) begins expanding first interaction between each pair of electrons i, j in Legendre polynomials of the cosine of the angle w_{ij} between two vectors from the core to the respective electrons, so that:

$$\frac{e^2}{r_{ij}} = e^2 \sum_k \frac{r_{<}^k}{r_{>}^{k+1}} P_k(\cos w_{ij}) \quad (2.40)$$

where $r_<$ indicates the distance from the nucleus (origin) to the nearest electron, and $r_>$ represents the distance from the nucleus to the electron farthest. If we now use the addition theorem for spherical harmonics,⁴⁷ we have:

$$P_k(\cos w_{ij}) = \frac{4\pi}{2k+1} \sum_q Y_{kq}^*(\theta_i, \phi_j) = \sum_q (-1) \left(C_{-q}^{(k)} \right)_i \left(C_q^{(k)} \right)_j \quad (2.41)$$

That reduces to:

$$P_k(\cos w_{ij}) = (C_i^{(k)} \cdot C_j^{(k)}) \quad (2.42)$$

Thus, equation (2.39) can be written as:

$$\left\langle \tau S L J M \left| \sum_{i < j} \frac{e^2}{r_{ij}} \right| \tau' S' L' J' M' \right\rangle = \sum_k e^2 \left\langle \tau S L \left| \sum_{i < j} \frac{r_{<}^k}{r_{>}^{k+1}} (C_i^j \cdot C_j^{(k)}) \right| \tau' S' L' \right\rangle \quad (2.43)$$

To proceed with the previous equation there are two paths: one is the method of determining JC Slater,⁴² which is not very efficient, and the other is the method of operators of G. Racah.⁴⁴ The method of Racah is a continuation of the original work of E.U. Condon and G.H. Shorthley⁴⁸ to calculate matrix elements. B.R. Judd⁴⁵ presented an excellent review of the application of these tensor methods to the configurations $4f^N$. A summary of this theory will be discussed later.

2.5 OPTICAL PROPERTIES OF TRIVALENT IONS IN CRYSTALLINE AND AMORPHOUS SOLIDS

We saw earlier that one of the most important characteristics of lanthanide ions is that the electrons involved in optical transitions are shielded by $5s^2$ and $5p^6$ shells. This shield makes the positions of the different spectral lines resulting little affected by introducing the ion in a glassy or crystalline matrix. This means that the positions of the ion energy levels are relatively little affected by its environment and can, therefore, correlate with the positions of energy levels of the configuration of free ions $4f^N$.

Professor Dieke⁴⁹ drew a diagram of trivalent lanthanide ions in LaCl_3 , see figure 2.2. With this diagram we can identify different energy levels of trivalent lanthanide ions in a variety of glassy and crystalline matrices. For a free atom or ion spherical symmetry exists, and each level is $2J + 1$ times degenerate. However, if the ion is placed in a crystalline medium, spherical symmetry is lost, and each energy level is split as a result of the action of electric field (Stark effect) due to the ion environment. Generally, the ion environment has a well defined symmetry (of lower symmetry than the spherical), and the degree to which it removes the degeneracy $2J + 1$ depend on the symmetry point in the position where is the rare-earth ion. Figure 2.2 shows the energy levels diagram for rare earth ions, obtained by Dieke.

For a particular type of rare earth ion in a crystal or glass, the wavelength of each peak of absorption bands or luminescence depends on the different contributions to the energy of the Hamiltonian for each ion.

The Hamiltonian H for an ion immersed in crystalline or glassy matrix can be written as:

$$H = -\frac{\hbar^2}{2m} \sum_{i=1}^N \nabla_i^2 - \sum_{i=1}^n \frac{Ze^2}{r_i} + \sum_{i<j}^N \frac{e^2}{r_{ij}} + \sum_l \lambda_l \vec{l} \cdot \vec{s}_{lj} + \sum_{i=1}^N eV(r_i, \theta_i, \phi_1) \quad (2.44)$$

where:

$$H_{cc} = -\frac{\hbar^2}{2m} \sum_{i=1}^N \nabla_i^2 - \sum_{i=1}^n \frac{Ze^2}{r_i} \quad (\text{Hamiltonian central field free ion})$$

$$H_{ee} = \sum_{i<j}^N \frac{e^2}{r_{ij}} \quad (\text{Repulsive electrostatic interaction})$$

$$H_{so} = \sum_l \lambda_l \vec{l} \cdot \vec{s}_{lj} \quad (\text{spin-orbit interaction})$$

$$H_{pcc} = \sum_{i=1}^N eV(r_i, \theta_i, \phi_1) \quad (\text{crystal field perturbation})$$

Expression (2.44) can be written as:

$$H = H_{cc} + H_{ee} + H_{so} + H_{pcc} = H_o + H_{pcc} \quad (2.45)$$

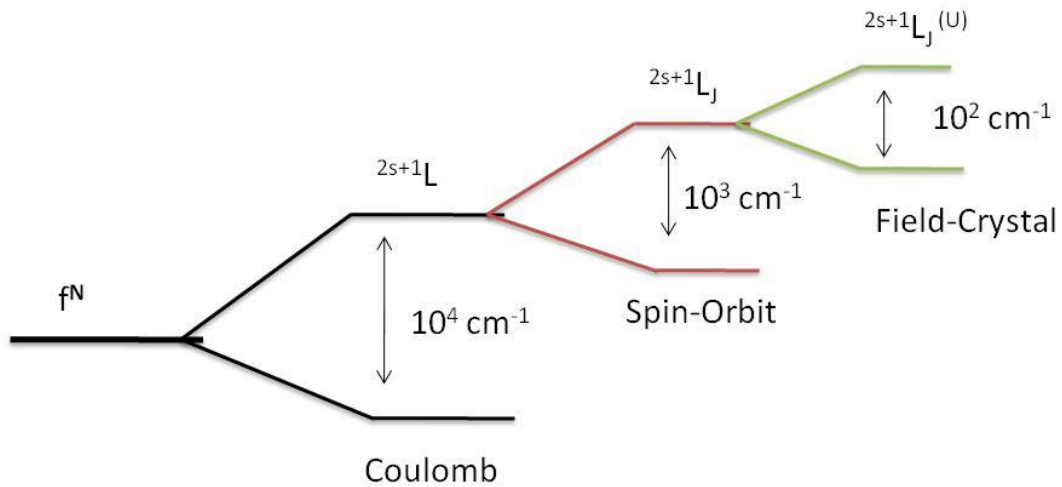
The first three terms contribute to the free ion Hamiltonian H_o , while the term H_{pcc} takes into account the effect of the crystal lattice over the energy levels of the ion. The diagonalization of the Hamiltonian (2.45) is a very complex task, so it is best to use approximate methods. Three cases may occur depending on the order of relative magnitude of different terms. The application of each case will depend on the type of ion:

- 1) $H_{pcc} > H_{ee} > H_{so}$ (strong crystal field approximation)
- 2) $H_{ee} > H_{pcc} > H_{so}$ (half crystal field approximation)
- 3) $H_{ee} > H_{so} > H_{pcc}$ (weak crystal field approximation)

The approximation of weak field crystalline is applied to rare-earth ions due to the shielding on the $5s^2 5p^6$ shells.

A schematic diagram of splitting of the energy levels in rare earth ions in glass and crystal is shown in figure 2.3.

Figure 2.3. Schema diagram of splitting of the energy levels of rare earth ions due to the different interactions.



Source: Author 2012.

3 JUDD-OFELT THEORY

3.1 Introduction to the Judd-Ofelt theory

The study of spectra of rare earth ions in glasses is an important focus of information that is normally used in various practical applications. Through these spectra we obtain information that, in principle, allows us to identify important electronic and vibrational frequencies of energy levels associated with the terminal stages of each of the excitations. Information obtained from the analysis of absorption spectra is essential for optical characterization of new materials of technology interest. Critical applications are associated, among others, to manufacture of lasers, optical fiber production at lower attenuation, and optical amplifiers. Spectral intensities of the electronic transitions of ions lanthanides have been approached using the Judd- Ofelt theory.^{45,46}

The static behavior of crystal field was a tremendous advance in understanding the radiative relaxation mechanisms, in the case of crystals and glasses doped with lanthanide ions. For these systems, the mechanism of intensities commonly used is the following: we assume that an f-f type excitation spectral intensity acquires transitions of the type f-d and/or f-g, where the static perturbation from odd components of the crystal field potential⁴⁵. This formalism was developed, assuming that the metal ions (M) and ion ligands (L) are separated by a distance sufficiently large to explicitly exclude the covering densities angular loads.⁴⁶ Consequently, the potential interaction is of long range (Coulomb) and charge transfer phenomena and others related, are outside the scope of the model.⁴⁶

In conclusion, we can say that: the Judd-Ofelt formalism was designed to explain the spectral intensities in different glassy and crystalline matrices doped with lanthanide ions incorporating only the crystal field contribution to electric dipole forces induced electronic transitions.

3.2 Hypothesis of the Judd-Ofelt theory

Electronic transitions between the f^N levels do not involve change in parity, so the electric dipole transitions are forbidden (Laporte rule). Such transitions become allowed if the odd harmonics static crystal field mixes states of opposite parities to the configuration $4f^N$. This can occur statically, if the rare earth ion is located at sites without inversion symmetry. This theory is based on the following hypothesis:

- The odd crystal field terms generated a mixture of electronic configurations of opposite parities that result the induced electric dipole mechanism.
- Differences in energy between two configurations are approximately equal to the energy difference between the barycenters of respective electronic configurations involved.
- All levels of the ground state are assumed equally populated.

The transitions observed in triply ionized rare earth ions are mainly of electric dipole nature, and only some contain significant magnetic dipole contributions. This observation is surprising at first, because the electric dipole operator:

$$P = -e \sum_i r_i \tag{3.1}$$

where e is the electrical charge of an electron and the sum runs over all electrons, has odd parity. Since all states inside a configuration possess the same parity, electric dipole transitions inside a configuration are forbidden, and with typical oscillator strengths around 10^{-6} the transitions are indeed relatively weak. We have mentioned above that, the occurrence and weakness of these transitions is explained by small admixing of other configurations with opposite parity to the ground configuration $4f^N$ by surrounding host material.

3.3 Quantitative analysis of Judd-Ofelt theory

Quantitative treatment of the intensities of absorption bands of trivalent lanthanides relates the experimentally determined oscillator strength, f_{exp} , and the theoretical model, which is based on the mechanisms by which radiation can be absorbed. The experimental oscillator strength can be obtained from the expression:⁵⁰

$$f_{exp} = \frac{[4.13 * 10^{-9}]}{Cl} \int \varepsilon(\sigma) d\sigma \quad (3.2)$$

where $\varepsilon(\sigma)$ is the optical density as a function of the transition energy (σ) in cm^{-1} , $C[mol/L]$ and $l[cm]$ are the concentration and the optical path respectively.

Theoretical oscillator strength of a spectral line corresponding to an electric dipole transition from one state $|A\rangle$ to an excited state $|B\rangle$ is given by the equation:

$$f = \left[\frac{8\pi^2 mc\sigma}{h} \right] \chi \left| \langle A | D_q^{(1)} | B \rangle \right|^2 \quad (3.3)$$

Where m is the electron mass, c is the speed of light, h is Plank's constant, σ is the (inverse of the wavelength, cm^{-1}), χ is the Lorentz field correction for the refractivity of the medium and $D_q^{(1)}$ the electric dipole operator. The matrix elements of electric dipole operator vanish between states from the same configuration.

In the previous chapter, Section 2.4, we mentioned that in the approximation of rare earth free ion, the configurations of the $4f^N$ states are taken as linear combinations of states cupped Russell-Saunders (RS) $|f^N \alpha SLJ\rangle$, such that:

$$|f^N \alpha [SL]J\rangle = \sum_{S,L} A(S,L) |f^N \alpha SLJ\rangle \quad (3.4)$$

where α represents all quantum numbers different from S , L , and J needed to completely specify the state. The wave function defined in equations (3.4) is frequently defined as $|f^N \psi J\rangle$.

The matrix electric dipole operator, vanishes between these states. To force an electric dipole transition is necessary to make a combination in the $4f^N$ configuration with another configuration of opposite parity. This combination may be obtained by the terms of odd parity of the crystal field expansion:

$$V^{C.F.} = \sum_{t,p} A_{t,p} D_p^{(t)} \quad (3.5)$$

with t odd. Considering the crystal field as a first-order perturbation, and as a combination of states for a configuration of opposite parity of higher energy, $|nl\alpha''[S''L'']J''\rangle$ (which will be written $|\psi''\rangle$), we can write $|A\rangle$ and $|B\rangle$ as follows:

$$|A\rangle = |f^N \psi J M\rangle + \sum_k \frac{\langle \psi'' | \langle f^N \psi J M | V^{C.F.} | \psi'' \rangle}{E(4f^N J) - E(\psi'')} \quad (3.6)$$

$$|B\rangle = |f^N \psi' J' M'\rangle + \sum_k \frac{\langle \psi'' | \langle f^N \psi' J' M' | V^{C.F.} | \psi'' \rangle}{E(4f^N J') - E(\psi'')} \quad (3.7)$$

in which k represents all the quantum numbers of the excited configuration. $E(4f^N J)$, $E(4f^N J')$, and $E(\psi'')$ are energy levels. Finally we can write the oscillator strength for a transition from state $|A\rangle$ to the final state $|B\rangle$ as:

$$f = \left[\frac{8\pi m c \sigma}{h} \right] \chi \left| \sum_{k,t,p} A_{t,p} \left\{ \frac{\langle f^N \psi_{JM} | D_q^{(1)} | \psi'' \rangle \langle \psi'' | D_p^t | f^N \psi' J' M' \rangle}{E(4f^N J') - E(\psi'')} \right. \right. \\ \left. \left. + \frac{\langle f^N \psi_{JM} | D_q^{(1)} | \psi'' \rangle \langle \psi'' | D_p^t | f^N \psi' J' M' \rangle}{E(4f^N J) - E(\psi'')} \right\} \right|^2 \quad (3.8)$$

and according to the Judd-Ofelt approximation, equation (3.8) can be written as:

$$f_{JJ'} = \frac{8\pi^2 m \sigma}{3 h e^2 (2J+1)} [\chi S_{ed}(JJ') + n S_{md}(JJ')] \quad (3.9)$$

where $\chi = (n^2 + 2)^2 / 9n$ is a factor for the effective field at a well-localized centre in a medium with an isotropic refractive index, m is the mass of the electron, e and h are de charge of the electron and Planck's constant, S_{ed} is the electric dipole line strengths, S_{md} is the magnetic dipole line strengths expressed respectively by⁵¹

$$S_{ed}(JJ') = e^2 \sum_{\lambda=2,4,6} \Omega_{\lambda} \langle \psi J || U^{\lambda} || \psi' J' \rangle^2, \\ S_{md}(JJ') = \left(\frac{e \hbar}{4 m c} \right)^2 \langle \psi J || L + 2S || \psi' J' \rangle^2 \quad (3.10)$$

where $||U^{\lambda}||$ are the doubly reduced matrix elements of the unit tensor operator of rank $\lambda = 2, 4, 6$ calculated from intermediate coupling approximation. The Ω_{λ} parameters are known as the Judd-Ofelt intensity parameters. They are closely related to the active ion environment and are given by:

$$\Omega_{\lambda} = (2\lambda + 1) \sum |A_{s,p}|^2 \Xi^2(s, \lambda) (2S + 1)^{-1} \quad (3.11)$$

in which the terms $|A_{s,p}|^2$ and $\Xi^2(s, \lambda)$ represent the crystal-field parameters and the nephelauxetic parameter β , respectively. The values of $\langle \psi_J || U^{\lambda} || \psi_{J'} \rangle^2$ were reported by Carnall *et al.*⁵². The Ω_{λ} parameters are determined by a least-squares fit of the theoretical oscillator strengths to the values of experimentally measured oscillator strengths calculated from optical absorption spectrum using equation (3.2).

The Ω_{λ} parameters are used to evaluate the radiative transitions rates (A_{rad}) from a particular emitting level according to the equation:

$$A_{rad}(J, J') = \frac{64\pi^4}{3h(2J + 1)\lambda^3} \times \left[\frac{(n^2 + 2)^2}{9} S_{ed} + n^3 S_{md} \right] \quad (3.12)$$

The radiative lifetime (τ_{rad}) of an emitting state and the emission branching ratio ($\beta_{JJ''}$) of a transition can be obtained by:

$$\tau_{rad}(J) = \frac{1}{\sum_{J'} A_{rad}(J, J')}$$

$$\beta_{JJ''} = \frac{A(J, J'')}{\sum_{J'} A_{rad}(J, J')} \quad (3.13)$$

In order to evaluate the validity of the intensity parameters, the deviation parameter is obtained by the root-means-square (rms, δ_{rms})

$$\delta_{rms} = \left[\frac{\sum f_{exp} - f_{cal}}{P} \right]^{1/2}$$

(3.14)

Where f_{exp} and f_{cal} are the experimental and calculated oscillator strengths, and P denotes the total numbers of levels used in the fitting procedure.

4 EXPERIMENTAL DETAILS

In this chapter, we present the investigated samples and spectroscopic properties of Nd^{3+} and Sm^{3+} doped solids (crystals and glasses) using the Judd-Ofelt Theory and conventional spectroscopy.

We have synthesized the following vitreous matrices doped with Sm^{3+} :

$38\text{InF}_3\text{-}20\text{SrF}_2\text{-}16\text{BaF}_2\text{-}20\text{ZnF}_2\text{-}2\text{GdF}_2\text{-}2\text{NaF-}2\text{SmF}_3$, acronym (Sm:InSrBaZnGdNa) and
 $34\text{InF}_3\text{-}20\text{SrF}_2\text{-}16\text{BaF}_2\text{-}20\text{ZnF}_2\text{-}2\text{GdF}_2\text{-}2\text{NaF-}2\text{SmF}_3\text{-XP}_2\text{O}_5$, acronym
(Sm:InSrBaZnGdNaPO).

The reagents used are of high purity 99.9%. These components were weighed and mixed in controlled atmosphere at temperature of 950 °C for one hour, thus is guaranteed their homogeneity after were melted in a platinum crucible at temperature of 950 °C for one hour, thus is guaranteed their homogeneity; after were dumped into a mold preheated to 270 ° C, avoiding thermal shocks , and finally bringing to room temperature. We obtained highly transparent glass with excellent optical quality.

Also, in this work were analyzed different glasses and crystal doped with Nd^{3+} and glasses doped with Sm^{3+} (table 4.1). All the glassy samples were synthesized by collaborators of the research group (Grupo de Fotônica e Fluidos Complexos – GFFC) of the IF-UFAL. Some crystals also were synthesized by collaborators and others acquired from manufacturers by means of donation or bought. In Table 4.1 we put all the investigated samples and the rare-earth concentrations.

Table 4.1 family of glasses and crystals with their respective acronyms and concentration % mol of earth rare (Nd³⁺, Sm³⁺)

Glass	Acronyms	x% mol	provider
Fluoroindate	Sm:InSrBaZnGdNa	2.0	[1]
Fluoroindate	Sm:InSrBaZnGdNaPO	2.0	[1]
Borate	Sm:BPbGeBi	1.0	[2]
Lead-Indium Phosphate	Nd:PbInPO ₄	1.0	[3]
Fluoroindate	Nd:InSrBaZnGdNa	1.0	[1]
Phosphate	Nd:Q-98	1.0	[4]
Phosphate	Nd:Q-98	4.0	[4]
Phosphate	Nd:Q-98	6.0	[4]
Phosphate	Nd:Q-100	10.0	[4]
Yttrium aluminoborate	Nd:YALB	0.75	[5]
Aluminosilicate	Nd:LSCAS	1.0	[6]
Borate	Nd:BNaPbAl	1.0	[7]
Borate	Nd:BNaPbAlTi	1.0	[7]
Y ₃ Al ₅ O ₁₂	Nd:YAG ceramics	1.0	[8]
Gadolinium Vanadate	Nd:GdVO ₄	1.0	[3]
Yttrium orthvanadate	Nd:YVO ₄	1.0	

Source: Author 2012.

[1] Grupo de Investigación em Materiales Fotónicos. UIS. Colombia.

[2] Instituto de Física de São Carlos-USP- Prof. Dr. A. S. S. de Camargo;

- [3] Universidade Federal do Ceará – Prof. Dr. Ilde Guedes;
- [4] Kigre Inc., Hilton Head, SC. Available at <http://www.kigre.com/glass.html>;
- [5] Instituto de Física de São Carlos-USP- Prof. Dr. A. C. Hernandez;
- [6] Universidade Estadual de Maringá – Prof. Dr. Mauro L. Baesso;
- [7] Universidade Federal de Uberlândia – Prof. Dr. Noélio Oliveira Dantas;
- [8] Universidade Autonoma de Madrid – Prof. Dr. Daniel Jaque

For some vitreous and crystalline samples were measured refractive index, and for this purpose we used an Abbe Refractometer NAR-4T ($n_D = 1.4700-1.8700; \pm 0.0002$) at wavelength of sodium (589 nm), using 1-bromonaphthalene contact liquid ($C_{10}H_7Br$). The density was calculated through the Archimedes method using a precise analytical balance Shimadzu AUW220D (0.1mg/0.01 mg), using distilled water as immersion liquid. The formula used was as follows:

$$\rho_g = \left[\frac{w_g}{w_g - w_a} \right] \times \rho_a \quad (4.1)$$

Room temperature absorption spectra in the ultra violet-visible-near infrared (UV-VIS-NIR) region for all the samples were recorded using high-performance spectrometer PerkinElmer LAMBDA 1050 with a spectral bandwidth of 0.5 nm.

To make a more systematic analysis, we begin the study with Sm^{3+} doped glasses and in the sequence we investigated the set of Nd^{3+} doped samples.

4.1 InSrBaZnGdNaSm AND InSrBaZnGdNaSmPO glasses doped with Sm^{3+} ion: influence of P_2O_5 in fluoroindate glass

The optical properties of the Sm^{3+} ions have been reported in a large number of glass systems.^{53,54,55} This ion has been of little interest and this is due essentially to two reasons: first because of the valence instability and the second due to the negative

values obtained from the Judd-Ofelt parameters for some glasses. Specifically in the case of fluoroindate glass, the Ω_2 parameter, obtained from the Judd-Ofelt theory, was negative⁵⁶, which is in contradiction with the definition of the parameters Ω_λ (in other words, this has no physical sense).

In accordance with the Judd-Ofelt approximation discussed in the chapter 3, this theory is applicable to cases where the high f-splitting is small as compared to the f-d energy gap since it is not appropriate to use in the high-energy levels for the calculation of the Ω_λ for case of Sm^{3+} ion. Despite these disadvantages, lately a variety of doped glass has emerged for multiple applications such as photodynamic therapy (PDT)⁵⁸ and substrate for CdTe solar cells⁵⁹ and they have been investigated/characterized using the Judd-Ofelt theory.

Judd Ofelt parameters obtained for $\text{Sm}:\text{InSrBaZnGdNa}$ and $\text{Sm}:\text{InSrBaZnGdNaPO}$ glasses doped with Sm^{3+} ion were obtained as follows: In present study were calculated the experimental oscillator strengths with the absorption spectra taking into account the physical parameters such as concentration, in *mol/l*, and thickness. The Ω_λ parameters are determined only for the low energy region and, for this, were used for each transition the matrix elements reported by Carnall.⁵⁷

The values of refractive index and mass density measured for the samples are shown in Table 4.2.

Table 4.2 Linear refractive index and mass density for $\text{Sm}:\text{InSrBaZnGdNa}$ $\text{Sm}:\text{InSrBaZnGdNaPO}$ glasses

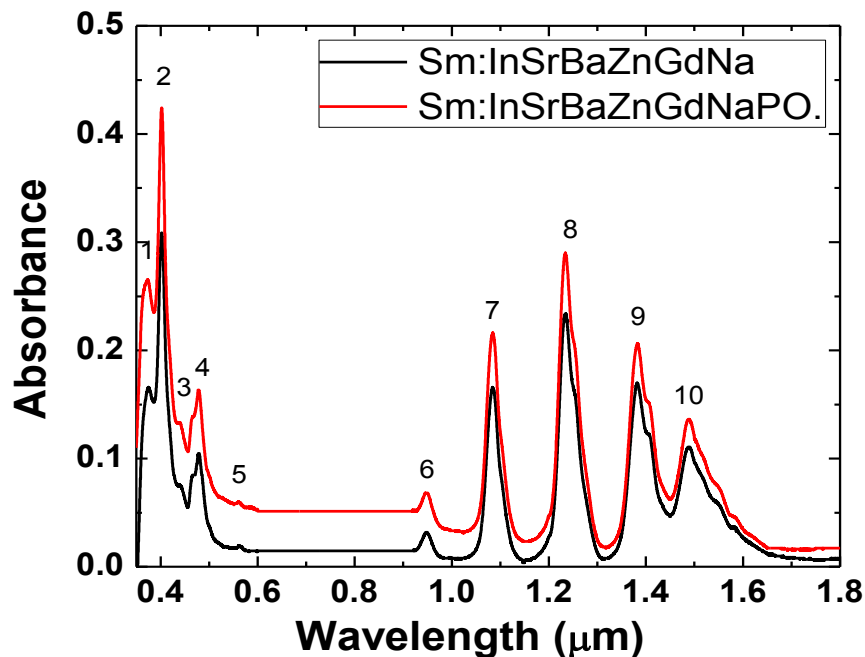
Glass system	Refractive index	Density [g/cm^3]
$\text{Sm}:\text{InSrBaZnGdNa}$	1.49	5.02
$\text{Sm}:\text{InSrBaZnGdNaPO}$	1.51	4.89

Source: Author 2012.

The Absorption spectra for $\text{Sm}:\text{InSrBaZnGdNa}$ and $\text{Sm}:\text{InSrBaZnGdNaPO}$, recorded in the range of 300 - 1800 nm and at room temperature, are shown in

Figure 4.1. The absorption spectrum shows 10 transitions from the ground state ${}^6H_{5/2}$ to each of the following energy levels (${}^6P_{7/2}, {}^4L_{17/2}, {}^4K_{13/2}, {}^4F_{9/2}$), ${}^4F_{7/2}, {}^4G_{9/2}, {}^4M_{15/2}, {}^4G_{5/2}, {}^6F_{11/2}, {}^6F_{9/2}, {}^6F_{7/2}, {}^6F_{5/2}, ({}^6F_{3/2}, {}^6H_{15/2}, {}^6F_{1/2})$. The majority of the transitions observed in the absorption spectrum are induced by electric dipole, with selection rules $\Delta J \leq 6$, but also occur transitions by magnetic dipole, specifically the transition ${}^6H_{5/2} \rightarrow {}^4G_{5/2}$.

Figure 4.1 Absorption spectra of 2.0 mol % of Sm^{3+} doped $\text{Sm}:\text{InSrBaZnGdNa}$ and $\text{Sm}:\text{InSrBaZnGdNaPO}$.



Source: Author 2012

The major difficult/problem in rare earths spectroscopy is the measurement/calculations of the intensities of absorption bands because in general occur overlap of the bands. The intensities of spectral lines are measured in terms of oscillator strengths. In the present work, the intensities of all the bands were calculated by the area method. Table 4.3 presents the experimental and calculated oscillator strengths for Sm^{3+} ions in InSrBaZnGdNa and InSrBaZnGdNaPO glasses. As can be observed, the calculated and experimental oscillator strengths are well consistent one with the other.

Table 4.3. Calculated and experimental oscillator strengths for Sm³⁺ doped InSrBaZnGdNa and InSrBaZnGdNaPO glasses.

Transitions	Sm:InSrBaZnGdNaPO		Sm:InSrBaZnGdNa	
	Oscillator strength (x10⁻⁶)			
	<i>f_{meas}</i>	<i>f_{cal}</i>	<i>f_{meas}</i>	<i>f_{cal}</i>
⁶ H _{5/2} → ⁶ F _{11/2}	0.22	0.34	0.21	0.32
⁶ F _{9/2}	2.08	2.09	1.96	1.97
⁶ F _{7/2}	3.07	3.02	2.86	2.84
⁶ F _{5/2}	1.48	1.50	1.43	1.42
⁶ F _{3/2}	0.73	0.73	0.68	0.67
		$\Delta f_{rms} = 0.08 * 10^{-6}$	$\Delta f_{rms} = 0.07 * 10^{-6}$	

Source: Author 2012

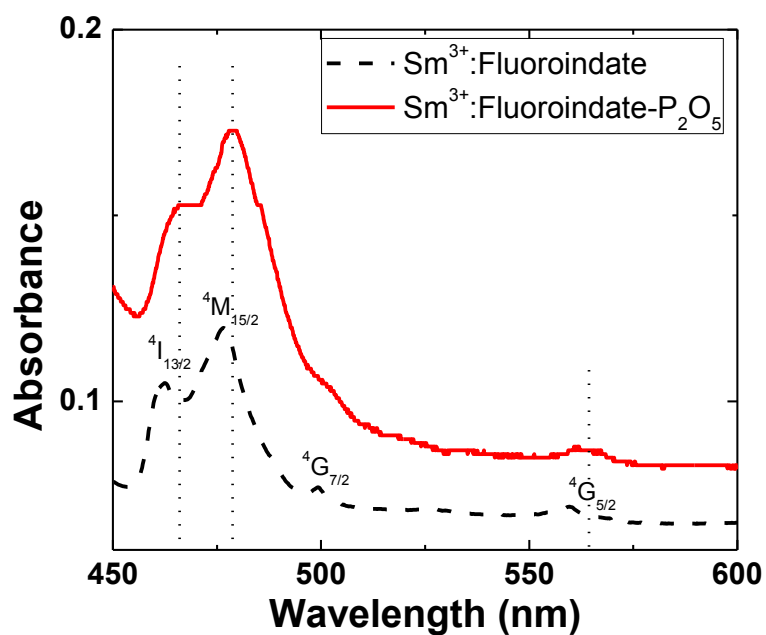
The table 4.4 shows the different matrix elements reported by Carnall for each transition observed in the absorption spectrum of the Sm³⁺ doped glasses. The presence of P₂O₅ in the fluoroindate glasses causes a small change in the molecular structure,⁶⁰ and this implies greater covalence between the Sm³⁺ ion and its ligands. The observed band shift, Figure 4.2, is due to the nephelauxetic effect⁶¹ that results in a contraction of the energy-level of rare-earth ions. This effect is caused by an overlap of the charge clouds of the ligands (in this case, oxygen atom) and the partly filled 4*f* shell of the Sm³⁺ ion.

Table 4.4. Energy levels assignments and matrix elements for Sm:InSrBaZnGdNaPO and Sm:InSrBaZnGdNa glasses

$S'LJ'$	$E_{exp} (cm^{-1})$		$U(2)$	$U(4)$	$U(6)$
	Sm:InSrBaZnGdNa	Sm:InSrBaZnGdNaPO			
${}^6P_{7/2}, {}^4L_{7/2}, {}^4K_{13/2}, {}^4F_{9/2}$	26795	26790	0	0.0025	0.0764
${}^4F_{7/2}$	24845	24846	0.0002	0.0012	0.0003
${}^4G_{9/2}$	22717	22717	0.0001	0.0010	0.0307
${}^4M_{15/2}$	20803	20802	0	0	0.0307
${}^4G_{5/2}$	17770	17762	0.0002	0.0007	0
${}^6F_{11/2}$	10573	10562	0	0.0006	0.0515
${}^6F_{9/2}$	9247	9221	0	0.0206	0.3413
${}^6F_{7/2}$	8130	8120	0.0020	0.1429	0.4301
${}^6F_{5/2}$	7256	7254	0.0332	0.2840	0
${}^6F_{3/2}, {}^6H_{15/2}, {}^6F_{1/2}$	6732	6728	0.3385	0.1365	0.0043

Source: Author 2012

Figure 4.2. Shift of transitions due to the nephelauxetic effect.



Fountain. Author 2012

4.1.1 Radiative properties of Sm:InSrBaZnGdNaPO and Sm:InSrBaZnGdNa glasses

The Judd-Ofelt parameters, Ω_2 , Ω_4 , and Ω_6 , electric dipole line strengths, radiative transition probabilities A_{rad} , branching ratio β_R , and radiative lifetime for Sm:InSrBaZnGdNa and Sm:InSrBaZnGdNaPO are shown in the tables 4.5 and 4.6.

The parameter Ω_2 is raised drastically by lowering the symmetry of rare earth ligand field. This parameters is more affected by the asymmetry of the crystal field and by changes of the energy difference between $4f^N$ and $4f^{n-1}5d$ configuration.

Table 4.5. Intensity parameters Ω_λ ($\times 10^{-20}$) ($\lambda = 2,4,6$) and quality factor Ω_4/Ω_6 for Sm:InSrBaZnGdNa and Sm:InSrBaZnGdNaPO glasses

Glass	Ω_2	Ω_4	Ω_6	Ω_4/Ω_6
Sm:InSrBaZnGdNa	0.03	2.90	2.46	1.17
Sm:InSrBaZnGdNaPO	0.07	2.99	2.56	1.16

Fountain. Author 2012

Table 4.6. Radiative decay rates $A_{rad}(s^{-1})$, branching ratio β_{rad} , and radiative lifetime $\tau_r(ms)$ for the main emitting states of Sm³⁺ doped InSrBaZnGdNa and InSrBaZnGdNaPO glasses.

Transition from $^4G_{5/2}$	$\Delta E(cm^{-1})$	InSrBaZnGdNaSm			InSrBaZnGdNaSmPO		
		A_{rad}	β_R	τ_r	A_{rad}	β_R	τ_r
$^6H_{11/2}$	14071	19.79	0.152	7.7	21.58	0.152	7.06
$^6H_{9/2}$	15442	31.49	0.242		34.98	0.247	
$^6H_{7/2}$	16993	74.98	0.578		81.30	0.574	
$^6H_{5/2}$	17770	3.42	0.026		3.77	0.026	

Source: Author 2012

4.2 Sm³⁺ doped BPbGeBi glass

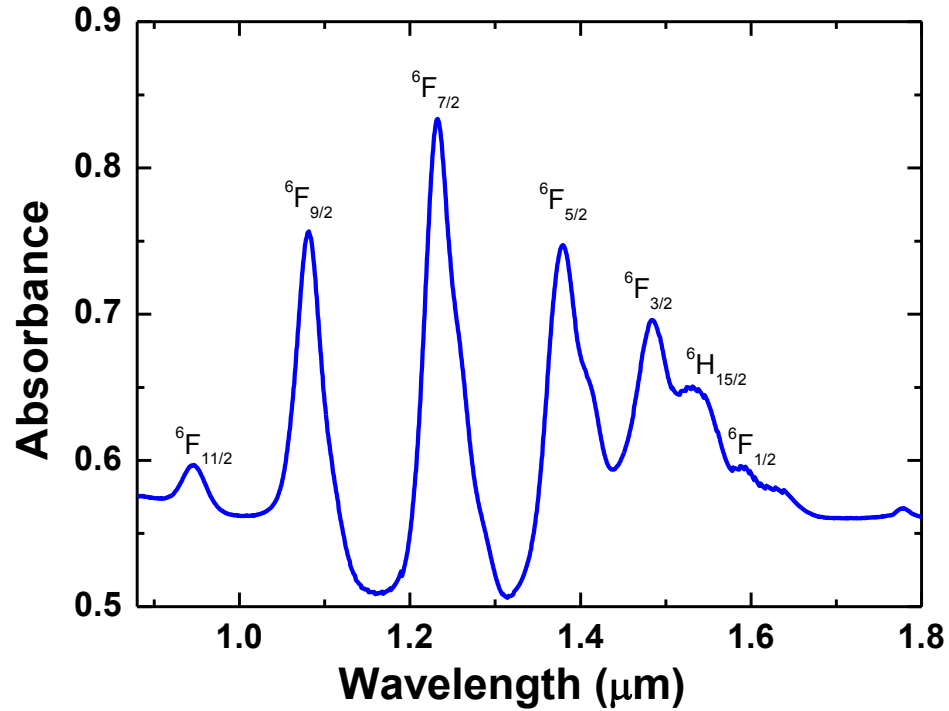
The sample used in this study has the following composition in (mol %): 26.66B₂O₃-52.33PbO-16GeO₂-4Bi₂O₃-1Sm₂O₃. It was prepared by the traditional melt-quenching technique in platinum crucible.⁶²

The Sm³⁺ doped BPbGeBi based glasses are of great interest for its wide transmission window, good thermal and optical properties, and possess high refractive indices (~1.80 – 2.2).⁶³ For this sample, the linear refractive index was found using the Foucault method,⁶⁴ and the obtained value was 1.93.

The absorption spectra occur due to the transition from the ground state ⁶H_{5/2} to various excited states ⁶F_{11/2}, ⁶F_{9/2}, ⁶F_{7/2}, ⁶F_{5/2}, ⁶F_{3/2}. Figure 4.3 shows the absorption spectrum of Sm³⁺ ion in BPbGeBi glass, at room temperature, in the spectral range from 800 to 1800 nm.

To study the Judd-Ofelt parameters of the Sm³⁺ ion in BPbGeBiSm glass, it was analyzed newly only for low energy regions, and the main important reasons for that is the existence of high absorption in the ultraviolet region by the presence of Bi³⁺ ions.

Figure 4.3. Optical absorption spectra of Sm^{3+} doped BPbGeBi glass



Source: Author 2012.

Conventional Judd-Ofelt theory has been used to perform analysis of the experimental absorption spectra. The reduced matrix elements $\|U^\lambda\|$ of the unit tensor operators necessary for calculations are listed in Table 4.7.

Table 4.7. Energy levels assignments and matrix elements for Sm:BPbGeBi glass

$S'L'J'$	$E_{exp} (cm^{-1})$	$U(2)$	$U(4)$	$U(6)$
${}^6F_{11/2}$	10564	0	0.0006	0.0515
${}^6F_{9/2}$	9221	0	0.0206	0.3413
${}^6F_{7/2}$	8116	0.0020	0.1429	0.4301
${}^6F_{5/2}$	7251	0.0332	0.2840	0
${}^6F_{3/2}, {}^6H_{15/2}, {}^6F_{1/2}$	6729	0.3385	0.1365	0.0043

Source: Author 2012.

The experimental and calculated oscillator strengths are shown in Table 4.8. The quality of the fitting is determined by the root means squared deviation (rms). The value of rms is in the typical error range of the Judd-Ofelt fitting and indicates good agreements between the experimental and calculated results. Ω_λ are important for investigation structure and transition properties of rare earths ions. The calculated values of $\Omega_2, \Omega_4, \Omega_6$ and quality factor Ω_4/Ω_6 in Sm:BPbGeBi glass is shown in the table 4.9.

Table 4.8. The experimental and calculated oscillator strengths for Sm^{3+} ions in BPbGeBi

Transitions	Oscillator strength ($\times 10^{-6}$)	
	f_{meas}	f_{cal}
${}^6\text{H}_{5/2} \rightarrow {}^6\text{F}_{11/2}$	0.36	0.48
${}^6\text{F}_{9/2}$	2.94	2.92
${}^6\text{F}_{7/2}$	3.92	4.00
${}^6\text{F}_{5/2}$	1.79	1.80
${}^6\text{F}_{3/2}$	0.28	0.31
$\Delta f_{rms} = 0.08 * 10^{-6}$		

Source: Author 2012

Table 4.9. Intensity parameters $\Omega_\lambda (\times 10^{-20})(\lambda = 2,4,6)$ and quality factor Ω_4/Ω_6 for Sm^{3+} doped BPbGeBi glasses.

Glass	Ω_2	Ω_4	Ω_6	Ω_4/Ω_6
Sm:BPbGeBi	0.6	2.44	2.52	0.96

Source: Author 2012

4.2.1 Radiative properties of Sm³⁺ DOPED BPbGeBi GLASS

The Table 4.10 shows the spontaneous transition probabilities, the branching ratio, and the radiative lifetime of the optical transitions in Sm:BPbGeBi glass.

Table 4.10 Radiative decay rates $A_{rad}(s^{-1})$, branching ratio β_{rad} , and radiative lifetime $\tau_r(ms)$ for the main emitting states of Sm³⁺ doped BPbGeBi glass

		Sm: BPbGeBi		
Transition from ${}^4G_{5/2}$ to	$\Delta E(cm^{-1})$	A_{rad}	β_R	τ_r
${}^6H_{11/2}$	14094	43.23	0.138	3.2
${}^6H_{9/2}$	15465	88.18	0.285	
${}^6H_{7/2}$	16716	172.06	0.550	
${}^6H_{5/2}$	17793	7.89	0.025	

Source: Author 2012.

4.3 Results and discussions

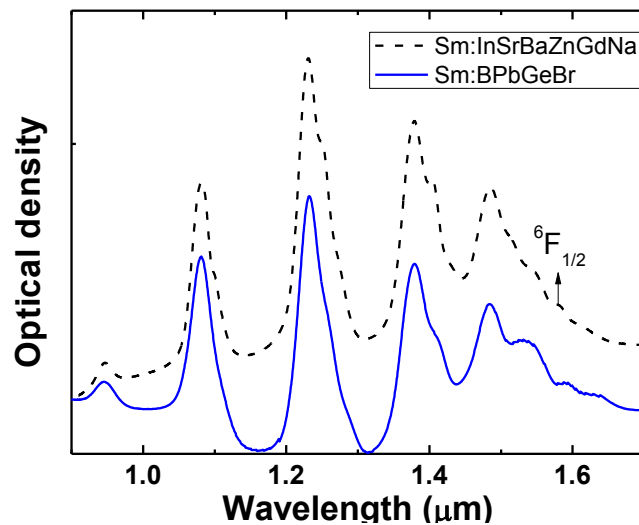
The majority of the transitions in the spectra originate from induced electric dipole interactions with selection rule $\Delta J \leq 6$. The ${}^6H_{5/2} \rightarrow {}^4G_{5/2}$ transition also contains magnetic dipole contribution with selection rule $\Delta J = 0, \pm 1$, ($\sim 0.08 \times 10^{-6}$) for fluoroindate glass.

Remembering the chapter four, the J-O parameters Ω_λ are closely related to the active ion environments given by the following expression:

$$\Omega_\lambda = (2\lambda + 1) \sum |A_{s,p}|^2 \Xi^2(s, \lambda)(2s + 1)^{-1} \quad (4.2)$$

where the terms $|A_{s,p}|^2$ and $\Xi^2(s,\lambda)$ represent the crystal field parameters and the nephelauxetic effect parameters, respectively. The $\Xi^2(s,\lambda)$ is proportional to nephelauxetic. Some authors have attributed such shifting to covalence of the host,⁶⁵ however, this has not yet been clearly ascertained with explicit generalized studies. For the glass Sm:BPbGeBi the parameter Ω_2 ($\sim 0.3 \times 10^{-20} \text{ cm}^2$) is high compared to the Ω_2 of the glasses Sm::InSrBaZnGdNa ($\sim 0.03 \times 10^{-20} \text{ cm}^2$) and Sm:InSrBaZnGdNaPO ($\sim 0.07 \times 10^{-20} \text{ cm}^2$). This can be explained through the nephelauxetic effect, where Jorgensen⁶⁵ interpreted as an expansion of the partly filled shell ($4f^{n-1}$ of RE ions) due to the transfer of the ligands to the core of the central RE^{3+} ion. The F^- ion due to its high electronegativity, small size, high charge density, and very small polarization, forms ionic bonds. The polarizability of the O^- anion by cations of the glass systems is greater than that of the F^- ion due to its comparatively larger size, greater charge and lower electronegativity. Consequently, metal-oxygen (M-O) bond has considerable covalent property with directional property. In present glasses, the peak wavelength of hypersensitive transitions, ${}^6\text{F}_{1/2}$, shifts towards longer wavelength for glass Sm:BPbGeBi. The figure 4.4 shows the hypersensitive transition for Sm:BPbGeBi and Sm:InSrBaZnGdNa glasses.

Figure 4.4 Hipersensitive transitions for Sm:BPbGeBi and Sm:InSrBaZnGdNa



Source: Author 2012

Nageno *et al.*⁶⁶ have studied alkali borate and phosphate glasses and concluded that the Ω_4 and Ω_6 parameters have a dependency with the viscosity and dielectric properties and are related to the rigidity of the glassy matrix. To make a more systematic study, we show in Table 4.11 the values for the Ω_λ ($\lambda = 2, 4, 6$) parameters found in the present work and others reported in the literature.

Table 4.11. Values for the Ω_λ ($\lambda = 2, 4, 6$) parameters and rigidity Ω_4/Ω_6 parameter for glasses studied in this work and some reported in the literature

Glass	Judd-Ofelt Parameter (10^{-20}cm^2)			Trend	Ω_4/Ω_6
	Ω_2	Ω_4	Ω_6		
Sm:InSrBaZnGdNa	0.03	2.90	2.46	$\Omega_2 < \Omega_6 < \Omega_4$	1.17
Sm:InSrBaZnGdNaPo	0.07	2.99	2.56	$\Omega_2 < \Omega_6 < \Omega_4$	0.96
Sm:BPbGeBi	0.6	2.44	2.52	$\Omega_2 < \Omega_4 < \Omega_6$	1.032
Sm:Tellurite ⁶⁷	0.001	0.34	0.24	$\Omega_2 < \Omega_6 < \Omega_4$	1.39
Sm:PbO-PbF ₂ ⁶⁸	1.16	2.60	1.40	$\Omega_2 < \Omega_6 < \Omega_4$	1.86
Sm:Phosphate ⁶⁹	4.31	4.28	5.78	$\Omega_2 < \Omega_4 < \Omega_6$	0.74

Source: Author 2012

It is remarkable to note that the order of the Ω_λ parameters is $\Omega_2 < \Omega_6 < \Omega_4$ for glasses Sm:InSrBaZnGdNa, Sm:InSrBaZnGdNaPo, Sm:Tellurite, Sm:PbO-PbF₂ and $\Omega_2 < \Omega_4 < \Omega_6$ for glasses Sm:BPbGeBi and Sm:Phosphate. The ratio Ω_4/Ω_6 in the glasses studied in this work (Sm:InSrBaZnGdNa, Sm:InSrBaZnGdNaPo, and Sm:BPbGeBi) are respectively 1.17, 1.16, and 1.032, being relatively rigid compared with Sm:Tellurite and Sm:PbO-PbF₂ glasses whose values are 1.39 and 1.86, respectively. Figures 4.5, 4.6, 4.7, and 4.8 show better the behavior of the Ω_λ ($\lambda = 2, 4, 6$) parameters and Ω_4/Ω_6 rigidity parameter as a function of the different matrices presented in table 4.11.

We mentioned earlier the nephelauxetic effect and its relation to the Ω_2 parameter. So, we proceed to calculate the value of the bonding parameter (δ), proposed by Sinha⁷⁰ through the following expression:

$$\delta = \left(\frac{1-\beta}{\beta} \right) \times 100 \quad (4.3)$$

Where β is the nephelauxetic effect expressed as follows:

$$\beta = (\sum_N \bar{\beta})/N \quad (4.4)$$

$\bar{\beta} = \frac{v_c}{v_a}$, where v_c and v_a are respectively the energies corresponding to the transitions in the investigated RE^+ in glass and free-ion in aqueous solution, and N denotes the number of levels used for the calculations of β values. Table 4.12 shows the values for $\bar{\beta}$ and δ .

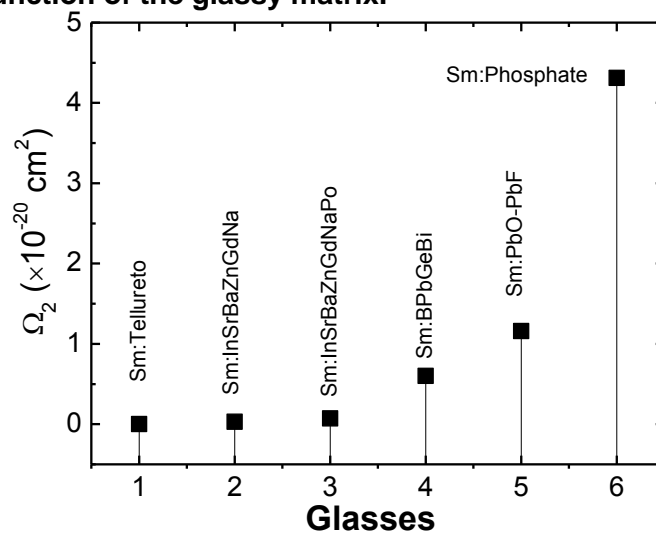
Table 4.12 Values of β and δ for Sm^{3+} doped glasses.

Glasses	β	δ	References
Tellurite	1.010126	-1.002	67
InSrBaZnGdNa	1.006232	-0.619	Present work
InSrBaZnGdNaPo	1.005001	-0.497	Present work
BPbGeBi	1.003546	-0.353	Present work
Phosphate	0.995792	0.4225	69

Source: Author 2012

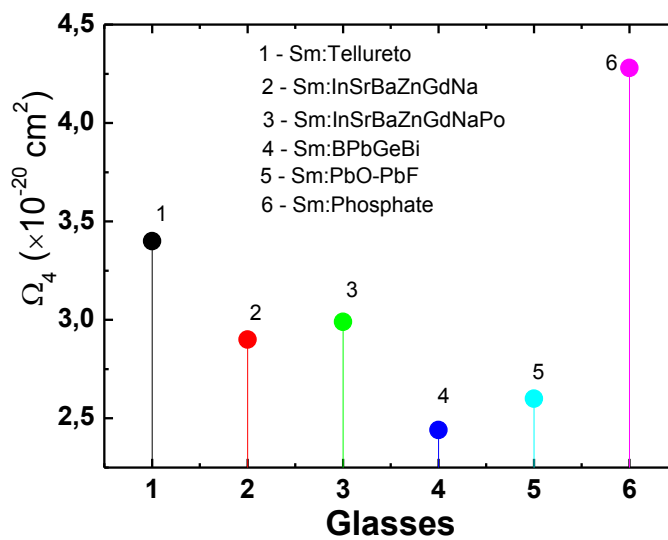
The lower value of the nephelauxetic parameter β for Phosphate glass indicates higher covalence in the Sm^{3+} -ligand bond. On the other hand, positive or negative values of the δ parameter indicate covalent or ionic bonding of the Sm^{3+} -ligand bond. Then, from the results presented in table we can infer that, for phosphate glass, which has higher Ω_2 parameter, has a significant covalent character compared to other glasses whose tendency is of ionic character.

Figure 4.5. Ω_2 as a function of the glassy matrix.



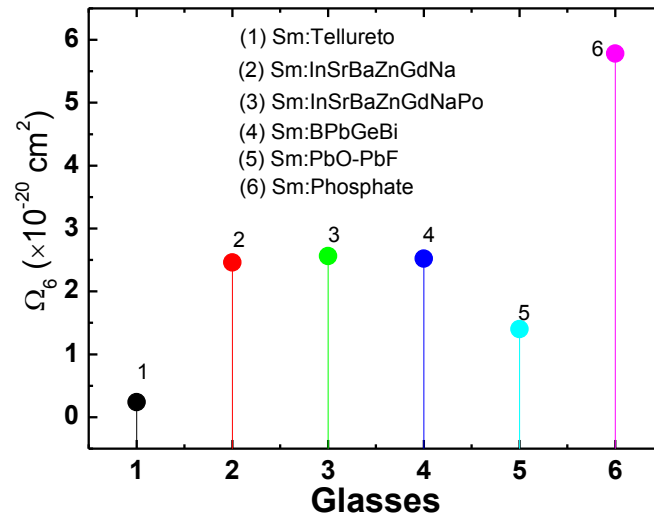
Source: Author 2012

Figure 4.6. Ω_4 as a function of the glassy matrix.



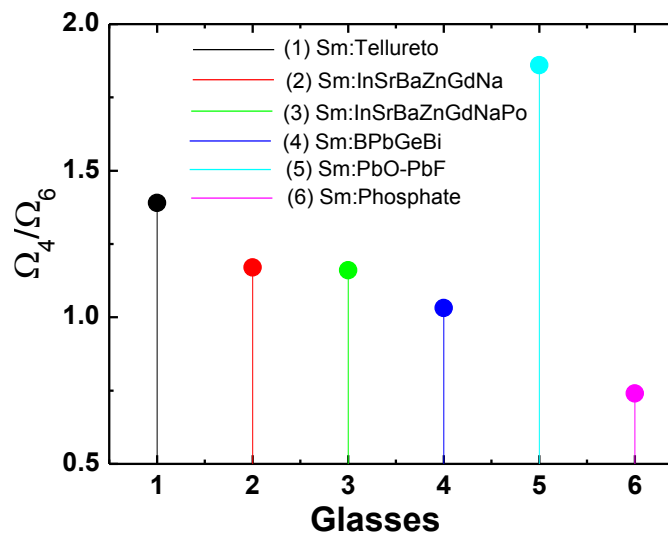
Source: Author 2012

Figure 4.7 Ω_6 as a function of the glassy matrix.



Source: Author 2012

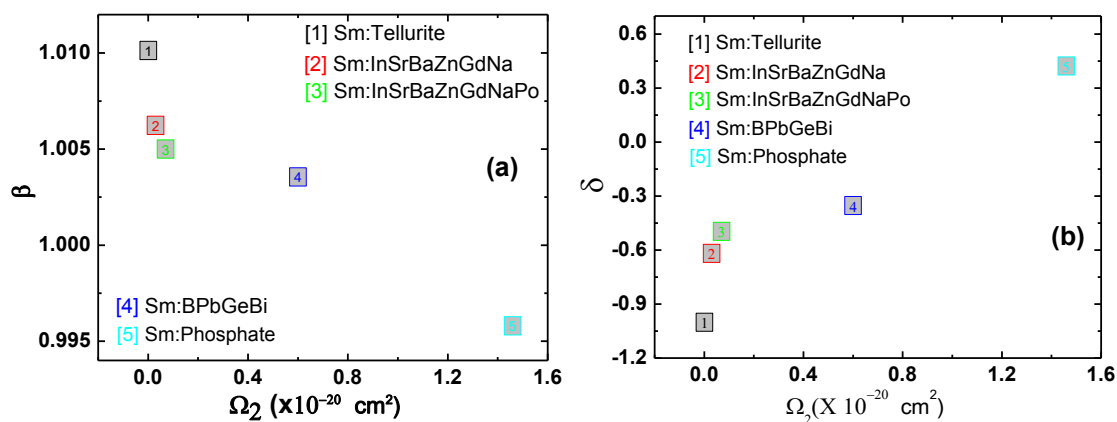
Figure 4.8 Ω_2/Ω_6 in function of the different glasses



Source: Author 2012

Figures 4.9 (a) and (b) show better the behaviors of the nephelauxetic $\bar{\beta}$ and δ parameters as a function of the Ω_2 parameter.

Figure 4.9 (a) β and (b) δ parameters as a function of the Ω_2 parameter



Source: Author 2012

From the figure 4.9, we can say that the nephelauxetic parameter characterizes the energy shift of these transitions with variations of glasses.

According to the above considerations, Ω_2 become larger with decreasing energy difference between 4f and 5d with is indicate by an increasing nephelauxitic parameters, this change explains the increase of Ω_2 due to increasing covalency at the RE sites.

Because Ω_6 is more dependent on changes of the electron density of the 4f and 5d orbitals, it is affected by covalency in a different way with respect to Ω_2 .

4.4 conclusions

Glasses having composition Sm:InSrBaZnGdNa, Sm:InSrBaZnGdNaPO , Sm:BPbGeBi have been prepared by melt quench technique.

Optical absorption spectra have been recorded. Judd–Ofelt approach has been applied for the f-f transition of Sm^{3+} ions to evaluate various intensity parameters Ω_2 , Ω_2 and Ω_6 . A good agreement is found between experimental and calculated oscillator strengths

Was observed that the hypersensitive transitions ${}^6\text{H}_{5/2} \rightarrow {}^6\text{F}_{1/2}$ is the most intense in Sm:BpbGeBi glass compared with glasses Sm:InSrBaZnGdNa, Sm:InSrBaZnGdNaPO, is probably due to the tendency of the covalency of the Sm ion and its environment.

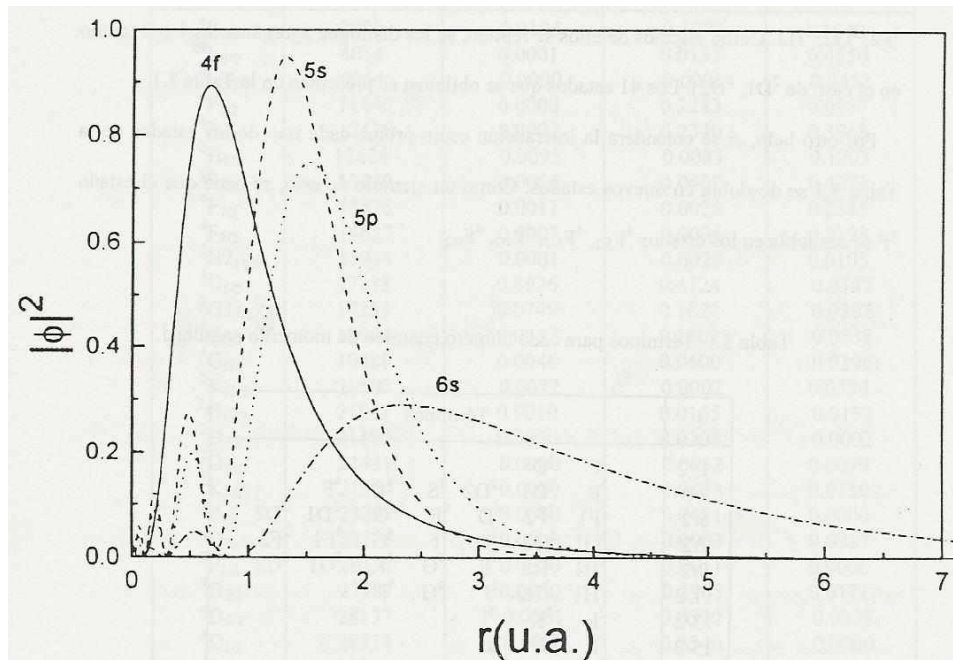
The low value of Ω_2 indicates the high symmetry around the rare earth ions and lower degree of covalence of rare earth–oxygen ions due to the lower mixing of opposite parity electronic configurations that are responsible of spectral intensities.

The radiative parameters such as Radiative decay rates $A_{rad}(s^{-1})$, branching ratio β_{rad} , and radiative lifetime $\tau_r(ms)$ of the ${}^4\text{G}_{5/2}$ emission level were calculated, the magnitude of branching ratio characterizes the lasing power of an emission transition and it is well established that an emission transition with branching ratio greater than 0.50 is more potential for laser emission, thus, the transition ${}^4\text{G}_{5/2} \rightarrow {}^6\text{H}_{7/2}$ exhibit values high of β_{rad} , being promising for laser applications.

4.5 Analysis of the Judd-Ofelt parameters and radiative properties of Nd³⁺ doped in glasses and crystal

We begin this section with a brief description of the Nd³⁺ ion and its importance in the use of laser devices. Nd ion is the most reactive rare earth and darkens rapidly on contact with air to form an oxide. It belongs to the family of internal transition elements and contains in its form stable 60 electrons. The Nd³⁺ ion has an ionic radius of 0.99 Å and its electronic configuration is of the form [Xe] 4f⁴6s², so that it contains only three electrons in the 4f shell (partially full). The wave functions of the f orbitals are under a screen effect of the wave functions corresponding to the sublevels 5s, 5p, and 6s (see Figure 4.10).

Figure 4.10. Radial wave functions of the 4f, 5s, 5p and 6s shells for Nd³⁺ ion



Fountain. Rare-Earth-Doped Fiber Lasers and Amplifiers

Due to this shielding effect, when the ion is placed in an external electric field (crystal field), it perturbs only slightly the 4f wave functions. If we use of the theory to sum the angular

momentum of the 4f electrons of the ion Nd^{3+} , considering one total angular momentum of spin S and one total orbital angular momentum L , we obtain 17 terms: 2P , 2D1 , 2F1 , 2G1 , 2H1 , 2I , 2K , 2L , 4S , 4D , 4F , 4G , 4I , 2D2 , 2F2 , 2G2 , and 2H2 . As some of these are repeated, they are distinguished by adding 1 or 2 (as in the case of 2D1 , 2D2). The 41 states that are obtained are presented in Table 4.13.

Table 4.13. Terms for each angular momentum quantum number J.

J	Terms							
1/2	2P	4D						
3/2	2P	2D1	2D2	4S	4D	4F		
5/2	2P	2F2	4D	4F	4G	2D1	2D2	
7/2	2G1	2G2	4D	4F	4G	2F1	2F2	
9/2	2H1	2H2	4F	4G	4I	2G1	2G2	
11/3	2H1	2H2	2I	4G	4I			
13/2	2I	2K	4I					
15/2	2K	2L	4I					
17/2	2L							

Source: Author 2012

On the other hand, considering the spin-orbit interaction, each of the states of Table 4.13 is split into new states. As an example we have the splitting of the 4f state in states ${}^4F_{3/2}$, ${}^4F_{5/2}$, ${}^4F_{7/2}$, and ${}^4F_{9/2}$. When the ion is in the presence of an electric field (crystal field), different states split to form doublets Kramer. The maximum multiplicity (number of lines of the multiplet) of each term is given in Table 4.14. The number of levels in which decomposes each term depends on the symmetry of the ion environment.

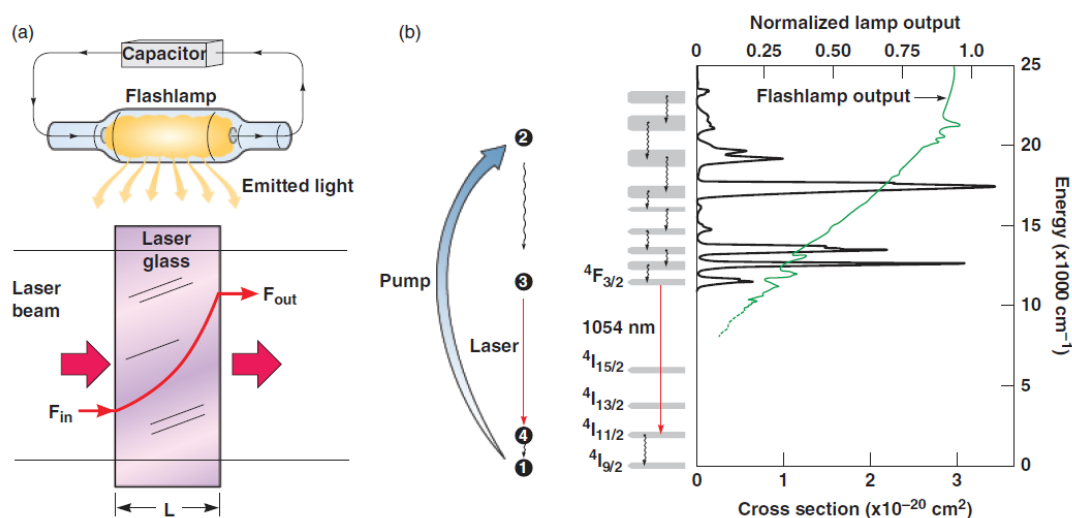
Table 4.14. Maximum multiplicity for each term

J	1/2	3/2	5/2	7/2	11/2	13/2	15/2	17/2
Degeneration	1	2	3	4	5	6	7	8

Source: Author 2012

In the range from 0 to 3000 cm^{-1} can be identified in the absorption spectrum around 15 bands. Its characteristic intensities can be observed for concentrations of about 1 or 2 mol% at room temperature, since for higher percentages may appear self-extinction effects in the emitted radiation. One of its main applications is as active medium in laser devices, taking as most relevant the Nd:YAG laser. In figure 4.11 we show a characteristic operation diagram for Nd^{3+} ion laser pumping.

Figure 4.11 a) Engineering and b) atomistic representations of flash-lamp pumping, Nd^{3+} excitation, and stimulated emission (amplification) in Nd^{3+} -doped laser.

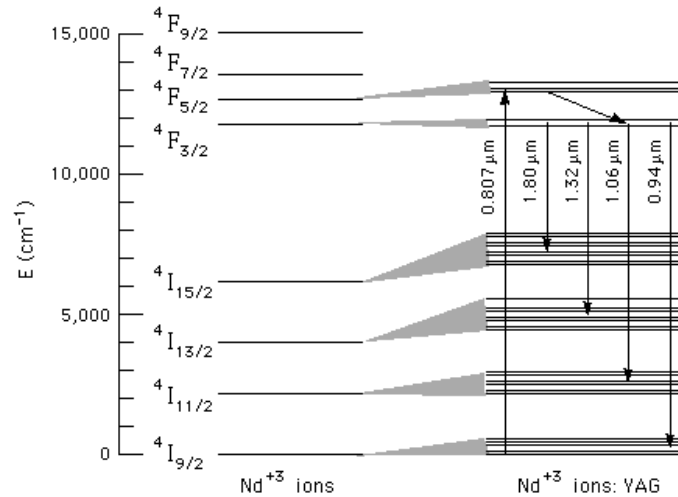


Source: International Journal of Applied Glass Science 2 [1] 3–29 (2011)

The transition ${}^4F_{3/2} \rightarrow {}^4I_{11/2}$ centered at $1,06\ \mu\text{m}$ has generated great interest due to its high intensity and quantum efficiency. Its most common application is in laser

devices of four levels, figure 4.12, using crystalline matrices such as YAG and YLF, and also amorphous such as phosphates and silicates.

Figure 4.12. Four-level system in Nd: YAG



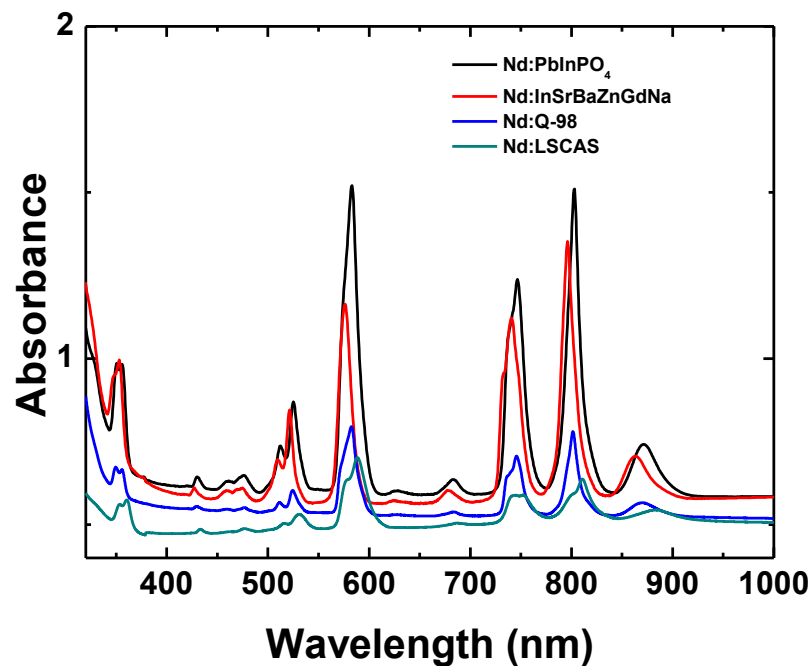
Source: Encyclopedia of Laser Physics and Technology

In this work we analyzed the absorption spectra of different Nd^{3+} doped glassy and crystalline matrices (see Table 4.1). So, following the same methodology developed for ion Sm^{3+} , we studied the Judd-Ofelt parameters and radiative properties.

4.5.1 Study of absorption spectra and calculation of Judd-ofelt parameters in different Nd^{3+} doped glasses

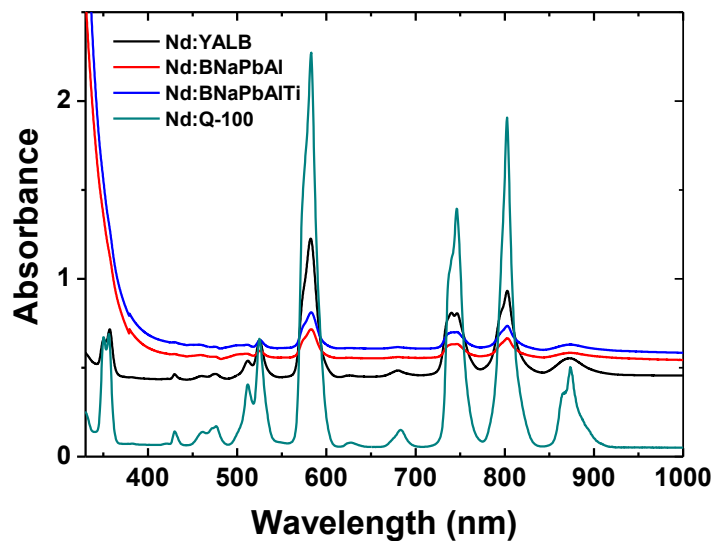
The absorption spectra of Nd^{3+} ions in Nd:PbInPO_4 , Nd:InSrBaZnGdNa , Nd:Q-98 , and Nd:LSCAS glasses are shown in figure 4.13 and of Nd:YALB , Nd:BNaPbAl , Nd:BNaPbAlTi , and Nd:Q-100 glasses in figure 4.14.

Figure 4.13. Absorption spectra of Nd:PbInPO₄, Nd:InSrBaZnGdNa, Nd:Q-98, and Nd:LSCAS glasses.



Source: Author 2012.

Figure 4.14. Absorption spectra of Nd:YALB, Nd:BNaPbAl, Nd:BNaPbAlTi, and Nd:Q-100 glasses.



Source: Author 2012.

Table 4.15 includes the transition from ${}^4I_{15/2}$ level identified in the studied spectral range and matrix elements of Carnall⁵⁷ for the Nd^{3+} ions and that were used in $Nd:PbInPO_4$, $Nd:InSrBaZnGdNa$, $Nd:Q-98$, $Nd:LSCAS$, $Nd:YALB$, and $Nd:Q-100$ glasses.

Table 4.15. J' states and matrix elements for Nd^{3+} ions and used in the $Nd:PbInPO_4$, $Nd:InSrBaZnGdNa$, $Nd:Q-98$, $Nd:LSCAS$, $Nd:YALB$, and $Nd:Q-100$ glasses

Upper state from ${}^4I_{9/2}$	Matrix elements		
	U_2^2	U_4^2	U_6^2
${}^4D_{3/2}, {}^4D_{5/2}^*, {}^2I_{11/2}, {}^4D_{1/2}$	0.0050	0.5257	0.0479
${}^2P_{1/2}^*, {}^2D_{5/2}$	0.0	0.0369	0.0021
${}^2K_{15/2}, {}^2G_{9/2}^*, ({}^2D^2P)_{3/2}, {}^4G_{11/2}$	0.0010	0.0441	0.0364
${}^2K_{13/2}, {}^4G_{7/2}^*, {}^4G_{9/2}$	0.0664	0.2180	0.1271
${}^4G_{5/2}^*, {}^2G_{7/2}$	0.9736	0.5941	0.0673
${}^4F_{9/2}$	0.0009	0.0092	0.0417
${}^4F_{7/2}, {}^4S_{3/2}^*$	0.0010	0.0449	0.6597
${}^4F_{5/2}^*, {}^2H_{9/2}$	0.0102	0.2451	0.5124
${}^4F_{3/2}$	0.0	0.2293	0.0549

Source: Author 2012.

For the case of $Nd:BNaPbAl$ and $Nd:BNaPbAlTi$ glasses, the matrix elements used are those shown in Table 4.16, this due to these glasses do not have high transparency in the UV-Vis region. Therefore, the bands ${}^4D_{3/2}, {}^4D_{5/2}^*, {}^2I_{11/2}, {}^4D_{1/2}$ are not displayed.

Table 4.16. J' states and matrix elements for Nd:BNaPbAl and Nd:BNaPbAlTi glasses.

Upper state from $^4I_{9/2}$	Matrix elements		
	U_2^2	U_4^2	U_6^2
$^2P_{1/2}^*, ^2D_{5/2}$	0.0	0.0369	0.0021
$^2K_{15/2}, ^2G_{9/2}^*, (^2D^2P)_{3/2}, ^4G_{11/2}$	0.0010	0.0441	0.0364
$^2K_{13/2}, ^4G_{7/2}^*, ^4G_{9/2}$	0.0664	0.2180	0.1271
$^4G_{5/2}^*, ^2G_{7/2}$	0.9736	0.5941	0.0673
$^4F_{9/2}$	0.0009	0.0092	0.0417
$^4F_{7/2}, ^4S_{3/2}^*$	0.0010	0.0449	0.6597
$^4F_{5/2}^*, ^2H_{9/2}$	0.0102	0.2451	0.5124
$^4F_{3/2}$	0.0	0.2293	0.0549

Source: Author 2012.

From the absorption spectra of each studied glass in this work, the experimental f_{exp} and calculated f_{cal} oscillator strengths were determined using equations 3.2 and 3.9. From the Tables 4.17 to 4.24 are presented the energies corresponding to each transition of Nd^{3+} ion for each glass analyzed in this work. The values of the experimental and calculated oscillator strength and their rms deviations are presented.

Table 4.17. Energy (cm^{-1}), experimental, and calculated oscillator strengths ($\times 10^{-6}$) for Nd:PbInPO₄ glass.

Energy (cm^{-1})	f_{exp}	f_{cal}
21015	0.26	0.45
19047	4.09	4.10
17140	11.80	11.76
14645	0.37	0.44
13394	5.54	5.68
12453	5.82	5.55
11454	1.64	1.78
$\delta_{rms} = \pm 0.12 \times 10^{-6}$		

Source: Author 2012.

Table 4.18. Energy (cm⁻¹), experimental, and calculated oscillator strengths (*10⁻⁶) for Nd:InSrBaZnGdNa glass

Energy (cm ⁻¹)	f_{exp}	f_{cal}
28248	5.71	5.96
23408	0.25	0.32
21052	1.27	0.78
19171	4.09	3.20
17349	7.50	7.50
14740	0.31	0.42
13487	5.12	5.59
12560	5.38	7.98
11574	1.36	1.30
$\delta_{rms} = \pm 0.51 \times 10^{-6}$		

Source: Author 2012.

Table 4.19. Energy (cm⁻¹), experimental and calculated oscillator strengths (*10⁻⁶) for Nd:Q-98 glass.

Energy (cm ⁻¹)	f_{exp}	f_{cal}
28121	6.98	7.37
23299	0.32	0.39
20990	1.32	1.09
19076	5.67	4.90
17164	18.13	18.16
14624	0.52	0.63
13408	7.60	8.35
12478	7.99	7.2
11502	2.16	1.65
$\delta_{rms} = \pm 0.26 \times 10^{-6}$		

Source: Author 2012.

Table 4.20. Energy (cm⁻¹), experimental, and calculated oscillator strengths (*10⁻⁶) for Nd:LSCAS glass.

Energy (cm ⁻¹)	f_{exp}	f_{cal}
27739	5.37	4.64
23068	0.25	0.25
20876	0.48	0.49
18850	2.24	2.44
16992	11.90	10.55
14556	0.25	0.22
13449	3.08	2.76
12338	3.37	2.78
11331	0.99	0.93
$\delta_{rms} = \pm 0.69 \times 10^{-6}$		

Source: Author 2012.

Table 4.21. Energy (cm⁻¹), experimental, and calculated oscillator strengths (*10⁻⁶) for Nd:YALB glass.

Energy (cm ⁻¹)	f_{exp}	f_{cal}
27996	19.61	19.89
23256	0.81	1.09
21052	2.53	2.37
19040	12.38	10.9
17170	40.78	40.85
14705	1.16	1.18
13509	14.47	15.00
12456	14.22	14.14
11455	3.36	4.10
$\delta_{rms} = \pm 0.33 \times 10^{-6}$		

Source: Author 2012.

Table 4.22. Energy (cm⁻¹), experimental, and calculated oscillator strengths (*10⁻⁶) for Nd:BNaPbAl glass.

Energy (cm ⁻¹)	f_{exp}	f_{cal}
23256	0.33	0.40
21052	0.72	0.86
19040	4.00	4.05
17170	15.16	15.11
14705	0.42	0.46
13509	5.62	5.74
12456	5.63	5.35
11455	1.55	1.53
$\delta_{rms} = \pm 0.03 \times 10^{-6}$		

Source: Author 2012.

Table 4.23. Energy (cm⁻¹), experimental, and calculated oscillator strengths (*10⁻⁶) for Nd:BNaPbAlTi glass.

Energy (cm ⁻¹)	f_{exp}	f_{cal}
23256	0.18	0.32
21052	0.54	0.70
19040	3.27	3.30
17170	12.24	12.21
14705	0.32	0.36
13509	4.66	4.73
12456	4.56	4.38
11455	1.26	1.24
$\delta_{rms} = \pm 0.07 \times 10^{-6}$		

Source: Author 2012.

Table 4.24. Energy (cm⁻¹), experimental, and calculated oscillator strengths (*10⁻⁶) for Nd:Q-100 glass.

Energy (cm ⁻¹)	f_{exp}	f_{cal}
28121	8.09	8.34
23299	0.36	0.45
20990	1.39	1.06
19076	5.54	4.77
17164	17.30	17.33
14624	0.49	0.55
13408	6.65	7.12
12478	6.90	6.50
11502	1.80	1.78
$\delta_{rms} = \pm 0.10 \times 10^{-6}$		

Source: Author 2012

4.5.2 Radiative properties of Nd³⁺ doped PbInPO₄, InSrBaZnGdNa, Q-98, LSCAS, YALB, BNaPbAl, BNaPbAlTi, and Q-100 glasses.

The Judd-Ofelt parameters obtained through the fitting between the measured f_{exp} and theoretical f_{cal} , for each studied Nd³⁺ doped glassy systems and spectroscopy quality factor are shown in table 4.25.

Table 4.25. Judd-Ofelt parameters ($\Omega_{\lambda} \times 10^{-20} \text{ cm}^2$), spectroscopy quality factor Ω_4/Ω_6 for Nd³⁺ doped PbInPO₄, InSrBaZnGdNa, Q-98, LSCAS, YALB, BNaPbAl, BNaPbAl, and Q-100 glasses.

Glass	Ω_2	Ω_4	Ω_6	$\frac{\Omega_4}{\Omega_6}$
Nd:PbInPO₄	5.08	3.89	7.39	0.52
Nd:InSrBaZnGdNa	1.32	2.37	4.16	0.56
Nd:Q-98	4.74	2.90	5.4	0.53

Nd:LSCAS	6.32	4.07	3.69	1.10
Nd:YALB	3.98	2.81	3.29	0.73
Nd:BNaPbAl	3.93	2.86	4.08	0.70
Nd:BNaPbAlTi	3.97	2.31	3.36	0.68
Nd:Q-100	4.48	2.72	5.55	0.49

Source: Author 2012

The Judd –Oflet parameters were used to calculate the electric-dipole line strength ($S_{ed}(JJ')$) corresponding to the transitions from the initial J manifold to the final J' manifold. For the Nd^{3+} ion, the emissions are a result of the following transitions: ${}^4F_{3/2} \rightarrow {}^4I_{15/2}$, ${}^4I_{13/2}$, ${}^4I_{11/2}$ and ${}^4I_{9/2}$. Once estimated ($S_{ed}(JJ')$), we proceed to obtain the radiative transitions rates (A_{rad}), expressed in equation 3.12, to finally obtain the radiative lifetime (τ_{rad}) and the emission branching ratio ($\beta_{JJ'}$), this latter given by equations 3.13. The values of these parameters are given in Table 4.26.

Table 4.26. Radiative properties such as radiative transitions rates A_{rad} (s^{-1}), radiative lifetime τ_{rad} (μs), and emission branching ratio $\beta_{JJ'}$ for Nd doped glasses.

Glass	$J \rightarrow J'$	A_{rad}	$\beta_{JJ'}$	τ_{rad}
Nd:PbInPO₄	${}^4F_{3/2} \rightarrow {}^4I_{15/2}$	13.21	0,004	362.35
	$\rightarrow {}^4I_{13/2}$	252.03	0,091	
	$\rightarrow {}^4I_{11/2}$	1357.87	0,492	
	$\rightarrow {}^4I_{9/2}$	1136.60	0,411	
Nd:InSrBaZnGdNa	${}^4F_{3/2} \rightarrow {}^4I_{15/2}$	10,447	0,005	558,75
	$\rightarrow {}^4I_{13/2}$	195,712	0,109	
	$\rightarrow {}^4I_{11/2}$	956,659	0,534	
	$\rightarrow {}^4I_{9/2}$	626,887	0,350	
Nd:Q-98	${}^4F_{3/2} \rightarrow {}^4I_{15/2}$	16.21	0.059	364.94
	$\rightarrow {}^4I_{13/2}$	321.15	0.117	
	$\rightarrow {}^4I_{11/2}$	1522.34	0.555	

	$\rightarrow^4I_{9/2}$	880.45	0.332	
Nd:LSCAS	$^4F_{3/2} \rightarrow ^4I_{15/2}$	8,276	0,0036	434.41
	$\rightarrow^4I_{13/2}$	161,018	0,0699	
	$\rightarrow^4I_{11/2}$	1012,716	0,4399	
	$\rightarrow^4I_{9/2}$	1119,921	0,4865	
Nd:YALB	$^4F_{3/2} \rightarrow ^4I_{15/2}$	10,719	0.005	482.72
	$\rightarrow^4I_{13/2}$	204,483	0.099	
	$\rightarrow^4I_{11/2}$	1057,417	0.510	
	$\rightarrow^4I_{9/2}$	798,956	0.386	
Nd:BNaPbAl	$^4F_{3/2} \rightarrow ^4I_{15/2}$	10.97	0.0053	481
	$\rightarrow^4I_{13/2}$	208.98	0.1005	
	$\rightarrow^4I_{11/2}$	1070.15	0.5147	
	$\rightarrow^4I_{9/2}$	788.86	0.3794	
Nd:BNaPbAlTi	$^4F_{3/2} \rightarrow ^4I_{15/2}$	9.03	0.0053	588.4
	$\rightarrow^4I_{13/2}$	172.108	0.1013	
	$\rightarrow^4I_{11/2}$	877.97	0.5166	
	$\rightarrow^4I_{9/2}$	640.382	0.3768	
Nd:Q-100	$^4F_{3/2} \rightarrow ^4I_{15/2}$	14.08	0.052	392.90
	$\rightarrow^4I_{13/2}$	266.70	0.105	
	$\rightarrow^4I_{11/2}$	1335.39	0.525	
	$\rightarrow^4I_{9/2}$	928.94	0.37	

Source: Author 2012.

4.5.3 Results and discussions

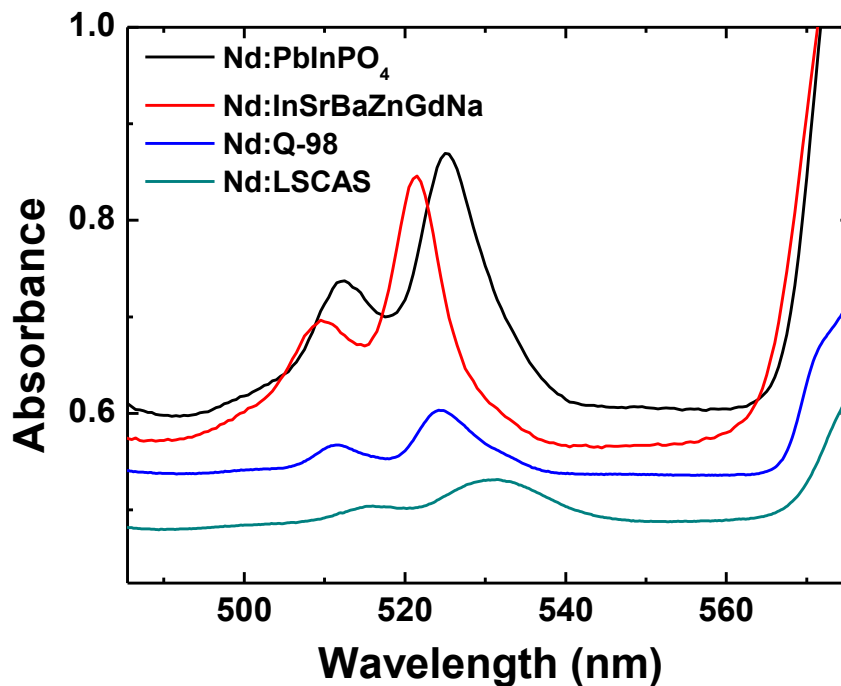
Experimental and theoretical oscillator strengths were obtained for all the studied glasses. In order to evaluate the validity of the intensity parameters, the deviation was obtained by root mean square δ_{rms} , thus obtaining a good fit for all samples. The obtained order for the JO parameters were:

- $\Omega_6 > \Omega_4 > \Omega_2$ for Nd:InSrBaZnGdNa;
- $\Omega_6 > \Omega_2 > \Omega_4$ for Nd:PbInPO₄, Nd:Q-98, Nd:YALB, Nd:BNaPbAl, Nd:BNaPbAlTi, and Nd:Q-100 glasses; and
- $\Omega_2 > \Omega_4 > \Omega_6$ for Nd:LSCAS glass.

The position and intensity of certain transitions are sensitive to the environment of the rare earth ion. These transitions follow the selection rules $\Delta J \leq 2$, $\Delta L \leq 2$ and $\Delta S = 0$. For Nd³⁺ ion the hypersensitive transition is the $^4I_{9/2} \rightarrow ^4G_{5/2} + ^2G_{7/2}$.

In Figure 4.15 is observed the shift in the barycenter of the glasses Nd-PbInPO₄, Nd:InSrBaZnGdNa, Nd:Q-98, Nd:LSCAS glasses for the hypersensitive transition. This shift indicated a change in the valence of the interaction between the Nd⁺³ and its immediate neighborhood formed by the ligand field.

Figure 4.15. Hypersensitive transitions observed for Nd:PbInPO₄, Nd:InSrBaZnGdNa, Nd:Q-98, and Nd:LSCAS glasses.



Source: Author 2012

We mentioned above that the Ω_2 Judd-Ofelt parameter indicates the covalent nature of the rare earth (RE) ion and ligand bond, as well as the asymmetric nature of

the Nd^{3+} ion local environment, i.e., the Ω_2 value varies according to the symmetry around the RE ion. Here, we did an analysis of the hypersensitive transition and nephelauxetic effect to have an idea on the nature of the Nd^{3+} and ligand bond. According to equations 4.3 and 4.4, we calculated the δ bonding parameter and nephelauxetic effect β and these results are shown in Table 4.27. As can be observed, the relative magnitude of δ indicate that the Nd^{3+} ions in LSCAS, PbInPO_4 , and Q-98 exhibit covalent character, since these values are positive. On the other hand, the negative value of δ for the InSrBaZnGdNa glass suggests an ionic character for this system.

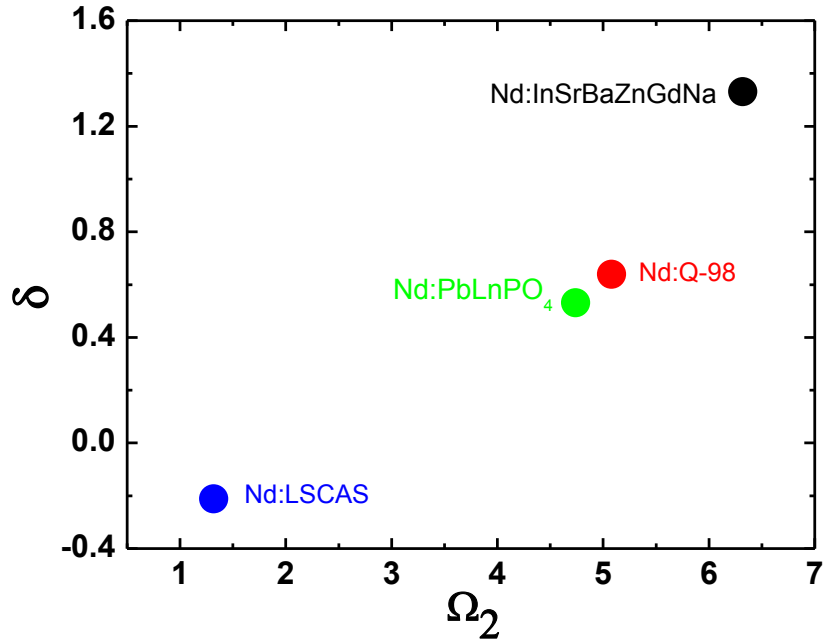
Table 4.27. Values of δ bonding parameter and Ω_2 Judd-Ofelt parameter for some Nd^{3+} doped glasses.

Glass	Ω_2	δ
Nd:LSCAS	6.32	1.331
Nd:PbInPO ₄	5.08	0.639
Nd:Q-98	4.74	0.530
Nd:InSrBaZnGdNa	1.32	-0.212

Source: Author 2012.

For a better visualization of the behavior, in Figure 4.16 we plot δ versus the Ω_2 parameter. Observing the graphs 4.15 and 4.16, we can conclude that, the shift can be understood in terms of the chemical bonding property of the ligands as a result of the overlap between the Nd^{3+} and ligands orbitals forming larger molecular orbitals, and knowing that the Ω_2 parameter is sensitive to the covalency,⁷² we can say that exist a dependent relationship between Ω_2 and δ parameters.

Figure 4.16. δ versus Ω_2 Judd-Ofelt parameter for four Nd³⁺ doped glasses.



Source: Author 2012.

It is known that the reduced matrix elements $\|U^2\|^2$ are zero and independent for ${}^4F_{3/2} \rightarrow {}^4I_J$ ($J=15/2, 13/2, 11/2, 9/2$). Hence the radiative properties depend only on Ω_4 and Ω_6 parameters because of the triangle rule $|J - J'| \leq \lambda \leq |J + J'|$.⁷³ Therefore, the spectroscopic quality factor Ω_4/Ω_6 , usually called Q and that was introduced by Jacobs and Weber, is in the range from 0.22 to 1.5 for Nd³⁺ doped in several host materials.⁷⁴ For all the samples analyzed in our study the quality factor is in this same range.

In literature is reported that for the case of $\Omega_4 \geq \Omega_6$, the efficiency of the ${}^4F_{3/2} \rightarrow {}^4I_{11/2}$ transitions is reduced while the ${}^4F_{3/2} \rightarrow {}^4I_{9/2}$ transitions are enhanced^{75,76}. From our results, the Nd:LSCAS glass present $\Omega_4 \geq \Omega_6$ (table 4.25), we observed that the transitions rates, A_{rad} , and emission branching ratio $\beta_{JJ'}$ is more enhanced for transitions ${}^4F_{3/2} \rightarrow {}^4I_{9/2}$.

4.5.2 Study of absorption spectra and calculation of Judd-Ofelt PARAMETERS Nd:YVO₄, Nd:GdVO₄ crystals and Nd: YAG ceramics

The crystals doped with Nd³⁺ have displayed be excellent materials for pumped lasers for commercial diodes primarily because presented intense absorption peaks around 800 nm, where the majority of the diodes emitting laser.

In recent decades, has been developed a increasing interest in laser crystals doped with Nd³⁺, due to its wide variety of technological applications, including as: integrated optical communication systems, high brightness devices, laser printers, and many other optoelectronic devices.

The YAG: Nd, remains the most common laser crystal for diode pumping. However, despite their wide use presents some important disadvantages. One of them is related to a phenomenon known as radiation extinction with increasing of the concentration ion(concentration quenching). This phenomenon of internal radiation extinction, requires that the concentration of the Nd³⁺ ion within the single crystal must have values close to 1% mol.

This relatively low concentration requires a large absorption length for the pumping light, and therefore require of great dimensions crystals, thus leading to significant internal losses (which are proportional to the length of the crystal). In addition to this, we have that the crystal growth process YAG: Nd is relatively expensive due to its high melting temperature (1960 °C)⁷⁷.

To avoid some of these problems, in recent years have been studied a series of new crystals doped with Nd³⁺ with lower melting temperatures, in order to obtain laser crystals that result not only more economical but also more efficient.

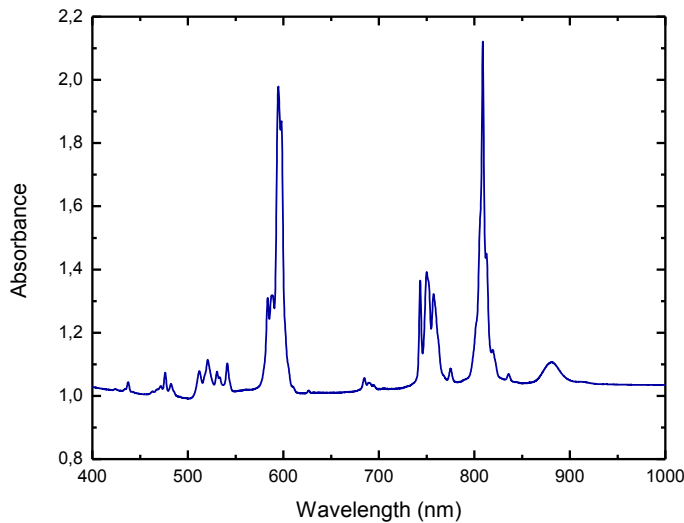
For this work we study the Judd Ofelt parameters and radiative properties for, Nd:YVO₄, Nd: GdVO₄ crystals and Nd:YAG ceramics.

4.5.2.1 Nd:YVO₄ crystal

Yttrium vanadate has been growing in popularity because of its high gain, low threshold, and high absorption coefficients at pumping wavelengths, which result from the excellent fit of the neodymium dopant in the crystal lattice. These advantages make Nd:YVO₄ is a better choice than Nd:YAG for low-power devices such as hand-held pointers, and others compact lasers.⁷⁸

The absorption spectra are shown on Figure 4.17

Figure 4,17 Absorption spectrum of Nd: YVO₄



Source: Author 2012

The table 4.28 shown the energy values, oscillator strength experimental and calculated for for Nd:YVO₄. RMS for the calculated oscillator strength is also given.

The parameters Judd- Ofelt Ω_{λ} ($\lambda = 2,4,6$) and spectroscopy quality $\left(\frac{\Omega_4}{\Omega_6}\right)$ for Nd:YVO₄ obtained is shown in the table 4.29.

Table 4.28 Experimental and calculated oscillator strengths ($\times 10^{-6}$) for Nd:YVO₄ crystal

Energy (cm ⁻¹)	f_{exp}	f_{cal}
22862	0.76	0.79
20999	4.05	3.98
20746	12.06	11.88
16812	41.30	41.29
14598	0.89	0.79
13333	14.16	15.23
12363	16.04	15.02
11350	2.85	2.56
$\delta_{rms} = \pm 0.13 \times 10^{-6}$		

Source: Author 21012

Table 4.29. Judd-Ofelt parameters ($\Omega_\lambda \times 10^{-20} \text{ cm}^2$) and the spectroscopic quality factor ($\frac{\Omega_4}{\Omega_6}$) for Nd:YVO₄.

Ω_2	Ω_4	Ω_6	$\frac{\Omega_4}{\Omega_6}$
5.35	3.38	4.44	0.76

Source: Author 2012.

With JO parameters obtained proceed to calculate the radiative lifetime (τ_{rad}) and the emission branching ratio ($\beta_{JJ'}$). The values of these parameters are given in Table 4.30.

Table 4.30. Radiative properties such as radiative transitions rates A_{rad} (s^{-1}), radiative lifetime τ_{rad} (μs), and emission branching ratio $\beta_{JJ'}$ for Nd:YVO₄

$J \rightarrow J'$	A_{rad}	$\beta_{JJ'}$	τ_r
${}^4F_{3/2} \rightarrow {}^4I_{15/2}$	26.36	0.005	195.72
$\rightarrow {}^4I_{13/2}$	511.37	0.101	
$\rightarrow {}^4I_{11/2}$	2635.74	0.515	
$\rightarrow {}^4I_{9/2}$	1935.84	0.378	

Source: Author 2012.

4.5.2.2 Nd:GdVO₄ crystal and Nd:YAG ceramic

In the last two decades have been developed diode pumped solid state laser. With the objective of improving and developing most efficient and high power compact laser, a wide variety of laser materials have been investigated.

The Nd: YAG laser has been widely studied for their optical properties and is the basis of the laser industry⁷⁹. It has a unique combination of spectral and laser properties also as high mechanical properties, thermal conductivity and has a wide optical transparency over a wide spectral region⁷⁹. However, it has certain limitations such as high cost and the ability to be doped with high concentrations of Nd, which is why, many investigations have focused in obtaining Nd: YAG systems for replace the traditional to have a high pump absorption efficiency⁸⁰.

Nowadays , many techniques have been developed to obtain new samples with the system Nd: YAG, such as crystal growth by thermal gradient, epitaxial thin-film deposition or ceramic technique⁸⁰, The latter is important because it is simple.

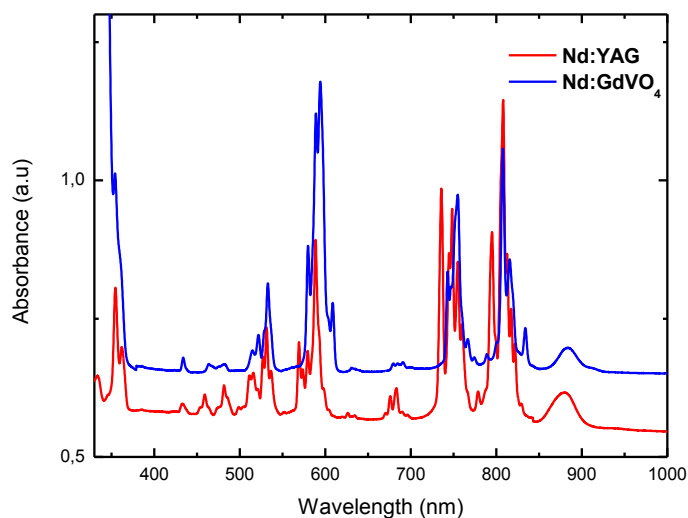
Nd-doped gadolinium orthovanadate (Nd:GdVO₄) crystal as a new laser material was first introduced in 1992⁸¹. It was discovered that Nd:GdVO₄ is a more efficient laser diode pumping solid state laser material than Nd:YVO₄ crystal.⁸²

The thermal conductivity of Nd:GdVO₄ is higher than that of Nd:YVO₄⁸³. The studies of other thermal properties of Nd:GdVO₄, such as thermal expansion and specific heat⁸⁴, show that Nd:GdVO₄ is suitable for high power laser system. It may be seen that Nd:GdVO₄ is more competitive than Nd:YVO₄ in high power laser generation.

Figure 4.18 shows the absorption spectra of Nd: YAG ceramic and Nd: GdVO₄ crystal.

The figure 4.18 shows that the Nd:YAG ceramic has a high Transmit window compared with that of GdVO₄ crystal in the region ultraviolet.

Figure 4.18. absorption spectra of Nd: YAG ceramic and Nd: GdVO₄ crystal.



Source: Author 2012.

Energy values, J' states, oscillator strength and matrix elements for Nd: GdVO₄ and Nd:YAG ceramic are shown in the tables 4.31 and 4.35 respectively.

Experimental and calculated oscillator strengths, Judd-Ofelt parameters

($\Omega_\lambda \times 10^{-20} \text{ cm}^2$), the spectroscopic quality factor ($\frac{\Omega_4}{\Omega_6}$), Radiative properties such as radiative transitions rates A_{rad} (s^{-1}), radiative lifetime τ_{rad} (μs), and emission branching ratio β_{JJ} for Nd: GdVO₄ crystal and Nd:YAG Crystal are shown in the tables 4.32, 4.33, 4.34, 4.37 and 4.38.

Table 4.31. Energy values, J' states, oscillator strength and matrix elements for Nd: GdVO₄

Upper state from $^4I_{9/2}$	Energy (cm ⁻¹)	Matrix elements		
		U_2^2	U_4^2	U_6^2
$^2P_{1/2}$	23052	0	0.0367	0
$^2K_{13/2}, ^4G_{7/2}, ^4G_{9/2}$	18761	0.0664	0.2180	0.1271
$^4G_{5/2}^*, ^2G_{7/2}, ^2H_{11/2}$	16829	0.9737	0.5968	0.0777
$^4F_{9/2}$	14484	0.0009	0.0092	0.0417
$^4F_{7/2}, ^4S_{3/2}^*$	13245	0.0010	0.0449	0.6597
$^4F_{5/2}^*, ^2H_{9/2}$	12382	0.0102	0.2451	0.5124
$^4F_{3/2}$	11310	0.0	0.2293	0.0549

Source: Author 2012

Table 4.32. Experimental and calculated oscillator strengths ($\times 10^{-6}$) for Nd: GdVO₄

Energy (cm ⁻¹)	f_{exp}	f_{cal}
23052	0.53	0.53
18761	6.71	5.97
16829	25.46	25.92
14484	0.34	0.60
13245	7.78	7.76
12382	6.81	7.38
11310	1.49	2,13
$\delta_{rms} = \pm 0.32 \times 10^{-6}$		

Source: Author 2012

Table 4.33. Judd-Ofelt parameters ($\Omega_\lambda \times 10^{-20} \text{ cm}^2$) and the spectroscopic quality factor ($\frac{\Omega_4}{\Omega_6}$) for Nd: GdVO₄ crystal

Ω_2	Ω_4	Ω_6	$\frac{\Omega_4}{\Omega_6}$
4.28	2.35	3.19	0.73

Source: Author 2012

Table 4.34. Radiative properties such as radiative transitions rates A_{rad} (s^{-1}), radiative lifetime τ_{rad} (μs), and emission branching ratio $\beta_{JJ'}$ for Nd: GdVO₄ crystal

$J \rightarrow J'$	A_{rad}	$\beta_{JJ'}$	τ_r
${}^4F_{3/2} \rightarrow {}^4I_{15/2}$	17,373	0,005	286,31
$\rightarrow {}^4I_{13/2}$	339,152	0,097	
$\rightarrow {}^4I_{11/2}$	1778,070	0,509	
$\rightarrow {}^4I_{9/2}$	1358,114	0,388	

Source: Author 2012

Table 4.35. Energy values, J' states, oscillator strength and matrix elements for Nd:YAG Ceramic

Upper state from ${}^4I_{9/2}$	Energy (cm^{-1})	Matrix elements		
		U_2^2	U_4^2	U_6^2
${}^4D_{3/2}, {}^4D_{5/2}^*, {}^2I_{11/2}, {}^4D_{1/2}$	28200	0.0050	0.5257	0.0479
${}^2P_{1/2}$	23105	0	0.0367	0
${}^2G_{11/2}$	21786	0.0	0.0053	0.0080
$({}^2D, {}^2P)_{3/2}, {}^2G_{9/2}, {}^2K_{15/2}$	20764	0.0010	0.0388	0.0284
${}^2K_{13/2}, {}^4G_{7/2}, {}^4G_{9/2}$	18818	0.0664	0.2180	0.1271
${}^4G_{5/2}^*, {}^2G_{7/2}$	16983	0.9736	0.5941	0.0673
${}^4F_{9/2}$	14632	0.0009	0.0092	0.0417
${}^4F_{7/2}, {}^4S_{3/2}^*$	13591	0.0010	0.0449	0.6597
${}^4F_{5/2}^*, {}^2H_{9/2}$	12376	0.0102	0.2451	0.5124
${}^4F_{3/2}$	11369	0.0	0.2293	0.0549

*Transition with greater contribution in the matrix elements.

Source: Author 2012

Table 4.36. Experimental and calculated oscillator strengths ($\times 10^{-6}$) for NdYAG Ceramic

Energy (cm^{-1})	f_{exp}	f_{cal}
28200	10.62	10.86
23105	0.38	0.54
21786	0.86	0.25
20764	1.39	1.12
18818	6.00	5.09
16983	7.62	7.71
14632	0.89	0.96
13591	8.92	8.78
12376	8.96	8.47
11369	1.62	2,30

$\delta_{rms} = \pm 0.27 \times 10^{-6}$

Source: Author 2012

Table 4.37. Judd-Ofelt parameters ($\Omega_{\lambda} \times 10^{-20} \text{ cm}^2$) and the spectroscopic quality factor ($\frac{\Omega_4}{\Omega_6}$) for Nd^{3+} for Nd:YAG Ceramic

Ω_2	Ω_4	Ω_6	$\frac{\Omega_4}{\Omega_6}$
0.22	3.10	5.34	0.58

Source: Author 2012

Table 4.38. Radiative properties such as radiative transitions rates A_{rad} (s^{-1}), radiative lifetime τ_{rad} (μs), and emission branching ratio β_{JJ} for Nd:YAG ceramic

$J \rightarrow J'$	A_{rad}	$\beta_{JJ'}$	τ_r
${}^4F_{3/2} \rightarrow {}^4I_{15/2}$	22.87	0,005	246,11
$\rightarrow {}^4I_{13/2}$	427.68	0,105	
$\rightarrow {}^4I_{11/2}$	2161.45	0,532	
$\rightarrow {}^4I_{9/2}$	1451.079	0,357	

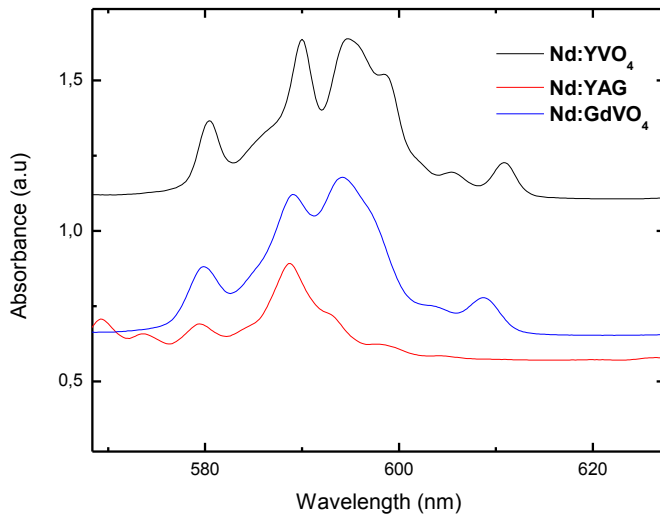
Fountain. Author 2012

4.5.3 Results and discussions

The transitions ${}^4I_{9/2} \rightarrow {}^4G_{5/2}$ have dependence strongly on the matrix elements U^2 . for our study for crystals, $|U^2|^2 = 0.9736$, thus, the parameters Ω_2 will be determined almost entirely by the absorbance of the ${}^4I_{9/2} \rightarrow {}^4G_{5/2}$ bands.

In Nd:YVO₄, this absorbance is larger than in the Nd:GdVO₄ and Nd:YAG ceramic, figure 4.19, which is reflect by the larger value of Ω_2 .

Figure 4.19. Absorption band for the transition ${}^4I_{9/2} \rightarrow {}^4G_{5/2}$ for Nd:YVO₄ and Nd:GdVO₄ and Nd: YAG crystal.



Source: Author 2012.

The size of parameter Ω_2 is important in determining the pumping efficiency of a Nd-laser crystal at the wavelength of the ${}^4I_{9/2} \rightarrow {}^4G_{5/2}$ transition, ≈ 580 nm, since the solar spectrum peaks near 500nm, in this work the values obtained for the parameter Ω_2 (10^{-20} cm^2) were: 5.35 for Nd:YVO₄, 4.28 for Nd:GdVO₄ and 0.22 for Nd:YAG

ceramic, so that, Nd:YVO₄ would be more efficient in solar pumping scheme than Nd:GdVO₄ and Nd:YAG ceramic.

The quality factor $\frac{\Omega_4}{\Omega_6}$ is larger in Nd:YVO₄ compared with Nd:GdVO₄ crystal and Nd:YAG ceramic, indicating that the Nd:YVO₄ crystal possesses more rigidity.

The transition ${}^4F_{3/2} \rightarrow {}^4I_{11/2}$ has only dependence of Ω_4 and Ω_6 , in order to maximize the probability of the emission in this transition, The quality factor $\frac{\Omega_4}{\Omega_6}$ should be as small as possible⁸⁵, in this work, the smallest value of $\frac{\Omega_4}{\Omega_6}$ is for Nd: YAG ceramic, indicating that the laser emission for the transitions ${}^4F_{3/2} \rightarrow {}^4I_{11/2}$ is relatively more intense.

4.5.4 Conclusions.

The optical properties of Nd:Q-98, Nd:Q-100, Nd:YALB, Nd:LSCAS, Nd:BNaPbAl, Nd:BNaPbAlTi, Nd:YAG ceramics, Nd:YVO₄ have been studied as a function of Judd-Ofelt intensity parameters.

Studying the parameter Ω_2 in different glassy matrices and Crystals and ceramic, we can conclude that higher values of this parameters indicates its stronger Nd³⁺ ligand covalent bond and/or higher asymmetry around Nd³⁺ ions.

The radiative decay rates of Nd³⁺ emissions in ${}^4F_{3/2} \rightarrow {}^4I_{J'}$ ($J'=9/2, 11/2, 13/2$ and $15/2$) are dominated by Ω_4 and Ω_6 , since the matrix elements $|U^2|^2 = 0$ for these transitions.

For the hypersensitive transitions ${}^4I_{9/2} \rightarrow {}^4G_{5/2}$, the parameter Ω_2 plays an important role, since the matrix element $|U^2|^2$ is high for this transition.

A higher branching ratio β value in Nd:YAG, signifies a higher stimulated emission cross section and consequently the ${}^4F_{3/2} \rightarrow {}^4I_{11/2}$ transitions is the widely used lasing transitions.

5 CONCLUSIONS AND PERSPECTIVES

5.1 Conclusions.

It was synthesized Sm:InSrBaZnGdNa and Sm:InSrBaZnGdNaPO glasses of high quality and homogeneity. The addition of P₂O₅ in the composition Sm:InSrBaZnGdNa increased the refractive index of the material, which is essential for laser applications. The optical properties of Sm:InSrBaZnGdNa, Sm:InSrBaZnGdNaPO, Sm:BPbGeBi, Nd:Q-98, Nd:Q-100, Nd:YALB, Nd:LSCAS, Nd:BNaPbAl, Nd:BNaPbAlTi, Nd:YAG ceramics, Nd:YVO₄ and GdVO₄ crystals were investigated basically using the Judd-Ofelt theory.

The values of experimental oscillator strength f_{exp} and calculated oscillator strength f_{cal} have been estimated. For each of the glasses and crystals investigate in this work the intensity parameters Ω_λ were calculated by a standard least square fitting and entirely analyzed. The variations in Ω_2 was discussed in terms of de covalent nature of the interaction between RE³⁺ (Nd³⁺, Sm³⁺) ion and the ligand field of the glass matrix.

The presence of the F⁻¹ ions plays the important role for the reduction of Ω_2 value. It is well known, the fluorine ions have the highest electronegativity (~4) in comparison with the other anion ions. Therefore, the RE-f bonds have ionic character and this is the main reason for the reduction of the Ω_2 values in the fluoride compounds.

The parameter Ω_4 presents a completely random behavior being, therefore, not easy to understand it.

Reasonably higher radiative property of ${}^4G_{5/2} \rightarrow {}^6H_{7/2}$ transition suggests that the Sm:InSrBaZnGdNa, Sm:InSrBaZnGdNaPO, Sm:BPbGeBi glasses are suitable candidates for reddish-orange laser applications.

The shift of the hypersensitive band of Sm:BPbGeBi glass (${}^6\text{H}_{5/2} \rightarrow {}^6\text{F}_{1/2}$; 1588 nm), with respect to the same transition of Sm:InSrBaZnGdNa glass, shows that the covalence of the RE–O bond increases, and this is due to the increased interaction between rare earth ions and its environment.

Radiative transitions rates (A_{rad}), branching ratio ($\beta_{JJ'}$), and radiative lifetime (τ_{rad}) were calculated for Sm:InSrBaZnGdNa, Sm:InSrBaZnGdNaPO, Sm:BPbGeBi, Nd:Q-98, Nd:Q-100, Nd:YALB, Nd:LSCAS, Nd:BNaPbAl, Nd:BNaPbAlTi, Nd:YAG ceramics, Nd:YVO₄ and GdVO₄ crystals. The obtained results enhance the usefulness of the glass and crystal system in optical displays, memory devices and laser.

In relation to the Nd:YVO₄, it would be a better solar-pumped laser candidate for space applications than Nd:YAG. It would also be more efficient than YAG when pumped by a dye laser (Rhodamine 6G).

5.2 Proposed future

From the results obtained in this work, goals for future works are:

1. The Judd-Ofelt parameters are useful for calculation of emission properties such as radiative decay rates, lifetimes and branching ratio of transitions. The comparison of calculated with experimental lifetime gives information about non-radiative decay rates. In the case of absence of non radiative decay processes as in the transition ${}^4\text{G}_{5/2}$ to the next lowest levels of Sm³⁺ ion, this process is purely radiative, since the energy difference between this level and the next lowest is 7250 cm⁻¹, thus, can be analyzed glasses and crystals doped with Sm³⁺, so be possible to assess the agreement between the Judd-Ofelt theory and experimental results.

2. Synthesize sets of silicate and borate glasses samples doped with Nd^{3+} ions modifying their structure, such that increase its ionic packing ratio, this with the objective of analyzing the behavior of Ω_6 .
3. Make an analysis of the Judd-Ofelt parameters in oxide and fluoride glasses doped with Nd^{3+} a function of the local basicity of the ligands.
4. Make a more detailed study of the decay rate as a function of the refractive index of glasses, so to try relate it to the parameter Ω_6 , since this parameter is more dependent on changes of the electron density of the 4f and 5d orbitals.

REFERENCES

1. Lidia Smentek, et al. Journal of Alloys and Compounds 323–324 (2001) 645–648
2. Liu G, Jacquier B (2005) Spectroscopic properties of rare earths in optical materials. Tsinghua
3. University Press & Springer, Beijing & Heidelberg C K & Judd B R, Mol Physics, 8 (1964) 281.
4. W. J. Miniscalco, "Optical and Electronic Properties of Rare Earth Ions in Glasses," in Rare-Earth-Doped Fiber Lasers and Amplifiers, Michel J. F. Digonnet, Ed. Marcel Dekker, Inc., New York, 17-112, 2001.
5. M. I. Ojovan (2004). ["Glass Formation in Amorphous SiO₂ as a Percolation Phase Transition in a System of Network Defects."](#)
6. Alexander Fluegel. ["Glass melting in the laboratory"](#). Glassproperties.com. Retrieved 2009-10-24.
7. Kerstin M. Forsberg, Ake C. Rasmuson, Crystallization of metal fluoride hydrates from mixed hydrofluoric and nitric acid solutions, Part I, Iron (III) and Chromium (III), Journal of Crystal Growth 312 (2010) 2351–2357.
8. R. Stepien, et al. Journal of Non-Crystalline Solids 357 (2011) 873–883.
9. Wei Fan, et al. Nature Materials 7, 984 - 991 (2008).
10. Olena Sych and Nataliya Pinchuk. Processing and Application of Ceramics 1 [1–2] (2007) 1–4.
11. Fuxi Gan, Optical and Spectroscopy Properties of Glasses, Springer-Verlag Publisher, Berlin, Heidelberg, 1992.
12. Charles, R. J. & Wagstaff, F. E. (1968). Journal of the American Ceramics Society, Vol. 51, 16-20.
13. I.A. BONDAR Institute of Silicate Chemistry of the USSR Acad. Sci. Leningrad, USSR. Rare-Earth Silicates. CERAMICS INTERNATIONAL, Vol. 8, n. 3. 1982.
14. J.H. Choi, et al. Adv. OptoElectron. 39892 (2007) 1–8.
15. E.S. Shepherd, G. A. Rankin, F. E. Amer. J. Sci, 1909. 28(4th): p. 293-333.
16. Pecoraro É, et al. Quím. Nova vol.23 n.2 São Paulo Mar./Apr. 2000

17. K. Suzuya, et al. Argonne National Laboratory. Oak Ridge National Laboratory. The Structure of Lead-Indium Phosphate Glass. 1994.
18. Hafner, et al. J. Am. Ceram. Soc. 1958, 41,315.
19. Hai Lin, et al. J. Of Lumin. 113, (2005), p 121–128.
20. D. Ruter, W. Bauhofer Appl. Phys. Lett., 69 (1996), p. 892.
21. M. Poulain, et al. Fluoride Glass Fiber Optics. Academic Press, New York, 1991, p. 1.
22. Y. Messaddeq, These de Doctorat, University of Rennes, France, 1990.
23. [Y. Messaddeq](#) et al. [J non-Cryst Solids](#) 161, pp. 210-212, (1993).
24. Yariv, Amnon (1989). Quantum Electronics (3rd ed.). Wiley. p. §10.3, pp. 208–211.
25. Geusic, J.F, et al, Appl. Phys. Lett., 4 p-182 (1964).
26. <http://www.cryslaser.com/news1/433.htm>.
27. A. I. Zagumenny, et al. 1992 . J. Quantum Electron. 22 1071.
28. [Y.-F. Chen](#) and [Y.P. Lan](#). Applied Physics B. [74, Numbers 4-5](#) (2002), 415-418.
29. [V. Lupei](#), et al. Optics Letters. 28 pp. 2366-2368 (2003).
30. H. R. Xia et al . J. Appl. Phys. 90, 4433 (2001).
31. Cillié, G. G. Monthly Notices of the Royal Astronomical Society, Vol. 96, p.771.
32. Edward Uhle et al, The Theory of Atomic Spectra,(Cambridge at the University Press, 1970).
33. L.Y. Shiff, Quantum Mechanics, Third Ed. Mc Graw- Hill, (1968).
34. Robert D. Cowan, The Theory of Atomic Structure and Spectra (Univ. California press) Vol I and Vol II.
35. Di Bartolo Baldassare, Optical Interactions in Solids, Ed. Wiley (1968).
36. A.S. Davydov. Quantum Mechanics. Pergamon Pr; 2 edition (June 1976).
37. Charlotte Froese Fischer. The hartree-Fock methods for Atoms: A Numerical Approach. John Wiley & Sons Inc. June 8, 1977.
38. [L.D. Faddeev](#) , [L.A. Khalfin](#) , [I.V. Komarov](#), V.A. Fock - Selected Works: Quantum Mechanics and Quantum Field Theory. CRC Press; 1 edition (May 21, 2004).
39. Karl A. Gschneidner, Jr., LeRoy Eyring, G.H. Lander and G.R. Choppin.

- Handbook on the Physics and Chemistry of Rare Earths, volume 18. Elsevier 1994.
40. A. Szabo, N.S. Ostlund. Modern Theoretical Chemistry MacMillan Pub. Inc., New York (1982).
 41. [George B. Arfken](#), et al. Mathematical Methods for Physicists. Academic Press, 17/01/2012.
 42. [Albert Messiah](#). Quantum Mechanics. Dover Publications, 06/07/1999.
 43. [Russell, H. N.](#); [Saunders, F. A.](#) Astrophysical Journal, vol. 61, p.38.1925
 44. G. Racah, [Phys. Rev. 63, 367 \(1943\)](#); [76, 1352 \(1949\)](#).
 45. B.R. Judd, Physical. Rev. 127 (1962) 750.
 46. G.S. Ofelt, J. Chem. Phys. 37 (1962) 511.
 47. John David Jackson. Classical Electrodynamics. John Wiley & Sons; 3rd Edition edition (1 Dec 1998)
 48. E. U. Condon and G. H. Shortley, The Theory of Atomic Spectra (Cambridge University Press, London, 1935)
 49. G.H. Dieke Spectra and Energy Levels of Rare Earth Ions in Crystals Wiley, New York (1968).
 50. K.A.Gschneider, L. Eyring , Handbook on the physics and Chemistry Of Rare Earts, 25, 167, 102-263 (1998).
 51. W.T. Carnall, et al. Handbook on the physics and chemistry of rare earth, Vol3. North-Holland,Amsterdam, 1987. Ch 24.
 52. W. T. Carnall et al, Chemistry Division, Report, 1967.
 53. Mierzejewski A, et al. J. Non-Cryst. Solids 104 323-32.
 54. Hairao K, et al, Opt. Lett. 18 1586
 55. Kurita A, et al. Opt. Lett. 19 314-6 (1994)
 56. A. Flórez, A. Herrera, M. Florez physica status solidi (c) [Volume 4, Issue 11](#), pages 4156–4164, November 2007.
 57. W. T. Carnall, et al. Chem. Phys. 49, 4424 (1968).
 58. B. J. Chen, et al. Optics Express, Vol. 20, Issue 2, pp. 879-889 (2012).
 59. [Stuedel, Franziska](#), et al. Proceedings of the SPIE, Volume 8438, pp. 843803-843803-7 (2012).

60. Joanna Pisarska, et al. *Physica B* 388 (2007) 331–336.
61. Som T et al. *Alloys Compounds* **476** 383–9 (2009)
62. FERNANDES R. G, et al. *Journal of physical chemistry. C*, v. 116, p. 6434-6445, 2012.
63. Katerina Knoblochova , et al. *Optical Materials* 31 (2009) 895–898.
64. Robert W. Wood, *Physical Optics*, 3^a. Ad. Optical Society of America, Washington, Dc, EUA (1988), pps. 70-72
65. C. K. Jørgensen, *Modern Aspects of Ligand Field Theory*, North-Holland, Amsterdam, 1971.
66. Y. Nageno, et al *J. Am. Ceram. Soc.* 76 (1993) 3081-3086
67. Akshaya Kumar, et al. *Spectrochimica Acta Part A* 59 (2003) 917_/925.
68. P. Nachimuthu, et al. *Non-Cryst. Solids* 217, 215 1997.
69. L. Boehm, R. et al. *J. Solid State Chem.* 28 (1979) 75
70. S.P. Sinha, *Complexes of the Rare Earth*, Pergamon Press, Oxford, 1966.
71. Bajaj A., et al. *Journal of Non-Crystalline Solids*, 355 (1) (2009) pp. 45-53.
72. R. Reifeld, *Struct. Bond.* 22 (1975) 123.
73. Y.C. Ratnakaram, N. Sudharani, *J. Phys. Chem. Solids* 59 (1998) 215.
74. R.C. Powell, *physics of Solid-State Laser Materials*, Springer, New York, 1998.
75. B. Viana, et al. *J. Non-Crystal. Solids* 215 (1997) 96.
76. M. Ajroud et al, *J. Phys.* 12 (2000) 3181.
77. Takunori Taira. *C. R. Physique* 8 (2007) 138–152.
78. D.G. Matthews, et al. *J. Modern Opt.* 43 (1996) 1079
79. W. Streck, A. et al. *Journal of Luminescence* 122–123 (2007) 70–73
80. Xiaorui Hou , et al. *Journal of Luminescence* 131 (2011) 1953–1958.
81. A. I. Zagumennyi, et al. *J. Quantum Electron.* **22**, 1071 (1992).
82. T. Jensen, et al. *Appl. Phys. B: Lasers Opt.* B58, 373 (1994)
83. P. A. Studenikin et al. *Quantum Electron.* 25, 1162 (1995).
84. H. Zhang, X. et al. *Mater. Res. Bull.* **34**, 1589(1999).
85. R.R. Jacobs, M. J. Weber, *IEEE J. Quantum. Electron*, 12 (1976) 102.